Extreme geomagnetic field variability indicated by Eastern Mediterranean full-vector archaeomagnetic records

P. Ertepinar[1], M. L. Hammond[2], M. J. Hill[3], A. J. Biggin[3], C. G. Langereis[1], A. I. R. Herries[4], K. A. Yener[5], M. Akar[6], , M.–H. Gates[7], T. Harrison[8], A. M. Greaves[9], D. Frankel[4], J. M. Webb[4], İ. Özgen[7], G. B. Yazicioglu[10]

1. Paleomagnetic Laboratory Fort Hoofddijk, Department of Earth Sciences, University of Utrecht, Budapestlaan 17, 3584 CD Utrecht, the Netherlands
P.Ertepinar@uu.nl
2. Sustrans Scotland, Rosebery House, 9 Haymarket Terrace, Edinburgh EH12 5EZ, UK
3. Geomagnetism Laboratory, Department of Earth, Ocean and Ecological Sciences, University of Liverpool, Liverpool L69 7ZE, UK.
4. The Australian Archaeomagnetism Laboratory, Department of Archaeology and History, La Trobe University, Melbourne Campus, Bundoora, 3086. VIC, Australia
5. Institute for the Study of the Ancient World, New York University, 15 East 84th St. New York, NY 10028, USA
6. Department of Archaeology, Faculty of Arts and Sciences, Mustafa Kemal University, 31060 Antakya, Hatay, Turkey
7. Department of Archaeology, Faculty of Humanities and Letters, Bilkent University, 06800 Bilkent, Ankara, Turkey
8. Department of Near and Middle Eastern Civilizations, University of Toronto, Toronto, Canada
9. Department of Archaeology, Classics and Egyptology, University of Liverpool, Liverpool L69 7WZ, UK.
10. Division of the Humanities, Near Eastern Languages and Civilizations, The University of Chicago, Chicago, Illinois 60637, USA

Abstract

The magnetic field of the Earth can exhibit considerable variations at short time scales, even as short as decades. The archaeomagnetic studies of Middle Eastern artefacts (mainly from Israel and Jordan) show evidence for an exceptionally high intensity period from 1050-700 BC which displays two distinct spikes over the Levant, the Levantine Iron Age Anomaly (LIAA). Its exact duration and geographical extent are still poorly known. Despite the wealth of ancient settlements, the extensive cultural heritage and a long history of trade and immigration, the archaeomagnetism of Turkey and Cyprus remains largely unexplored. This study presents a large data set of ancient directions and intensities from seven archaeological sites in the Eastern Mediterranean covering a time span of ~2000 years. The recorded directions from thirteen sets of samples are coherent with our earlier findings, yet

show significantly larger swings than existing field models. In particular, we confirm the very large swing in inclination we found earlier, from 1910-1850 BC, that is also captured by the Greek PSV curve, and shallower by more than 10° than predicted by existing field models. Consequently, these models require substantial revision in this region. We were able to determine the archaeointensity from five sets of mud-bricks, from the thirteen attempted, allowing us to provide the full field vector. Furthermore, we present thirty-one new archaeointensity results from potsherds and mud-bricks that considerably enhance existing data, especially when a set of strict selection criteria is applied. Fourteen sets of potsherds from a single site (Tell Atchana) provide the longest sequence recorded so far in Turkey, from 2100 to 1350 BC. We find exceptionally high intensities of 145 and 175 ZAm^2 around 700 BC, in well-dated mud-bricks and potsherds from two different locations (Tell Tayinat and Kilise Tepe), supporting extreme geomagnetic field variability in the region. Moreover, these two high intensities confirm the younger spike of the LIAA in Turkey.

Keywords: Archaeomagnetism, archaeointensity, Turkey, Cyprus, geomagnetic spike, Levantine Iron Age Anomaly

1. Introduction

Archaeomagnetism studies burnt or fired archaeological artefacts to help understand short term variations of the Earth's magnetic field (palaeosecular variation; PSV) over the last 8,000 years or so, PSV studies are important for understanding the geodynamo that maintains the Earth's magnetic field while good PSV curves for a region can help to date certain archaeological artefacts. Archaeological features that are commonly studied include *in-situ* features such as kilns, ovens and hearths, which can provide geomagnetic field directions and palaeointensity, and *ex-situ* artefacts like tiles, bricks and ceramics that can only be used for palaeointensity studies (Thellier and Thellier, 1959).

The importance of archaeomagnetism in revealing short term changes in the strength of the geomagnetic field, such as the Levantine High, has been highlighted in recent years by studies from Syria and Iran (Gallet et al., 2015, 2014, 2008, 2006; Gallet and Butterlin, 2015; Genevey et al., 2003; Stillinger et al., 2015), Jordan, Israel and Georgia (Ben-Yosef et al., 2017, 2009, 2008a, 2008b; Shaar et al., 2017, 2016, 2015, 2011), Turkey (Ertepinar et al., 2016, 2012), and Iraq and Cyprus (Shaar et al., 2015; Tema et al., 2018; Yutsis-Akimova et al., 2018a, 2018b). The focus of recent research has been on the Middle East between ~3000-0 BC partly because Gallet et al. (2006) suggested that PSV may have played a role in controlling climate, related to what they called four 'archaeomagnetic jerks' recorded in French and Middle Eastern data. An archaeomagnetic jerk was defined as a period of high field intensity coinciding with a sharp cusp in geomagnetic field direction (Gallet et al., 2003); it is also referred to as a 'geomagnetic spike' when the high field intensity periods occur in relatively short episodes (Ben-Yosef et al., 2009). The three oldest intensity highs are proposed to have occurred based on data from Syria and Iran (Gallet et al., 2006). The fourth and youngest interval at 1050-750 BC shows a significantly higher magnitude than the three older events and is now well-known as the 'Levantine Iron Age Anomaly (LIAA)' (Shaar et al., 2016). The LIAA was first discovered in the Southern Levant (Ben-Yosef et al., 2008a), and subsequently in Turkey (Ertepinar et al., 2012) and Georgia (Shaar et al., 2017). The LIAA is

seen as a short period of exceptionally high field intensities producing VADM (virtual axial dipole moment) values in excess of 200 ZAm^2, and appears to show two distinct spikes at ~980 BC and ~740 BC (Shaar et al., 2016). However, the spatial extent of the high intensity spike is still not well constrained. Currently available data do not yet allow determination of whether the LIAA is a rapid regional perturbation or is a global scale phenomenon, and whether it is represented by single or multiple high field episodes.

A better knowledge of the evolution of the geomagnetic field in space and time would allow a better understanding of geodynamo processes as well as enabling the construction of better field models and constraining regional PSV curves to establish the nature of such high field episodes. In order to acquire this knowledge, full vector field information is required from as many different locations and times as possible. There is still a lack of published work in this area centered in Turkey and Cyprus, despite their extensive cultural heritage and a long history of trade and immigration. Abundant Cypriot slag deposits have recently been exploited as a reliable recorder of the geomagnetic field and have the potential to provide a very high resolution time series (Ben-Yosef et al., 2008a; Shaar et al., 2010), However, the data from this region are still scarce. Spatially, Turkey and Cyprus (including the Mediterranean Sea) cover a very large area that is almost the same size as one third of Europe. Considering the scarcity of the data from the region, it is inevitable that geomagnetic field models are relatively unconstrained by local data and rely heavily on data published for Bulgaria (Kovacheva et al., 2014), Greece (De Marco et al., 2014; Tema and Kondopoulou, 2011) and the Middle East. This study presents a new and large dataset of palaeodirections and palaeointensities from archaeological sites in Turkey and Cyprus, spanning the time interval from 2700 to 750 BC, the period suggested to include at least four high intensity episodes. The results help to better constrain the LIAA (1050-700 BC) at ~750 BC, to narrow the data gap over Turkey and Cyprus, and to increase the accuracy of global field models.

2. Archaeological Context and Sampling

We have sampled seven archaeological sites, two in Cyprus and five in Turkey (Fig. 1). The Cypriot sample sets consist solely of potsherds while the sample sets from Turkey consist of both potsherds and oriented samples. All potsherd sets were selected from previously excavated collections. Dependent on the availability of material, we selected sets of potsherd samples containing 6-15 samples (but occasionally only 1 or 2) per archaeological context/level (Table 1a). For oriented samples, a water-cooled drill was used to take cylindrical cores of 2.5 cm diameter and a magnetic compass was used to orient the cores *in situ*. Cores were drilled at different orientations in order to detect any anisotropy effect if present. If core length permitted, more than 1 specimen was cut from the core. Oriented sample sets contain 7-36 samples and 7-46 individual specimens per age/level (Table 1b). The majority (fifteen) of the oriented sets are sampled from surfaces that were exposed to fire, such as destruction levels or fire places. The remaining five sets are from a stratigraphic sequence of palace pavements and made from manufactured mud-bricks. These palace pavement mud-bricks did not experience any subsequent fire event and would only have been baked (or sun-dried) during manufacture. They are sampled for palaeointensity measurements and inclination-only analysis (explained in detail in the following sections).

The age of the archaeological sites, contexts or level mostly rely on the ^{14}C dates, pottery typology and relative chronology. Below we briefly describe the sampling sites; detailed information and references are given in the Supplementary Material.

Bellapais Vounous (Cyprus). Six Red Polished Ware sherds (BV-P) have been studied here (Fig. S1); all date from the Early Cypriot I-II period (2250-2100 BC).

Marki Alonia (Cyprus). We studied twenty-eight pottery sherds with various typologies (MA-P) which have been taken from contexts dated between 2400-1900 BC (Fig. S1, Table S1).

Hacımusalar Höyük (Turkey). We sampled three different levels from ~3 m high North-South trending trench where HM1 (fallen mud-bricks) and HM2 (a clay pit) are the uppermost and lowermost destruction levels dating back to Early Iron (1200-1000 BC) and Early Bronze Ages (3300-2100 BC), respectively. The third level HM3 (mud-bricks) is stratigraphically between the two levels, closer to HM2 (Fig. S2).

Kilise Tepe (Turkey). We studied eight potsherds (KIT-P) from five different occupation levels over an age interval of 1350-30 BC (Fig. S3).

Kinet Höyük (Turkey). We collected two sets of mostly mud-brick (and some serpentinite) samples from the eastern terrace of the mound (KN1 and KN2) which date back to 2000-1750 BC and 1750-1550 BC (Fig. S4).

Tell Atchana (Turkey). The stratigraphy of Tell Atchana has been subdivided into a sequence of eighteen occupation levels (Level 0 to Level XVII/XVIII, 2200-1305 BC). We have chosen 128 potsherds (TA-P), from fourteen levels as being representative of the variety in pottery typology found on the site (Fig. S5a). We additionally sampled fourteen sets (mud-bricks, basalts and an ash layer) for the full vector analyses (Fig. S5b). Five of these sets belong to a stratigraphic sequence of levels of palace pavements that were analysed for both archaeointensity and inclination only, assuming that the bricks were horizontally fired during manufacture, instead of sun-dried. This assumption is tested in the following sections.

Tell Tayinat (Turkey). We collected one mud-brick set (TT1) from the burnt Iron Age II temple that was destroyed by an intense fire at ~672 BC (Fig. S6).

3. Rock Magnetic Experiments and Results

Rock magnetic properties such as the room temperature bulk susceptibility, Isothermal Remanent Magnetisation (IRM) acquisition, hysteresis loops, first order reversal curve (FORC) diagrams and Curie curves are measured using a Kappabridge KLY-2, an

alternating gradient force magnetometer, and a modified horizontal translation type Curie balance (Mullender et al., 1993).

The IRM experiment results on potsherds (Fig. 2a) indicate that all samples contain a low coercivity phase and are saturated in fields well below 300 mT. All curves except for one (BV-P) showed almost fully reversible heating curves if heated up to ~600°C; occasionally, some alteration (oxidation) occurred if heated to 700°C, producing a slightly lower intensity in the final cooling curve. All curves from BV-P, MA-P and TA-P have a change in slope at or close to 580°C, and hence the inferred dominant magnetic carrier is magnetite. Four of the eight KIT-P samples show two Curie temperatures (T_c), the first at ~300°C, the second at ~580°C implying the presence of both Ti-rich titanomagnetite and magnetite. Three of the other samples have curved thermomagnetic curves where it is impossible to isolate a T_c. The remaining one sample has a T_c of ~550°C due to the presence of Ti-poor titanomagnetite. These interpretations are supported by the low coercivities (B_c=6-14 mT) observed in the samples (Fig. 2a).

The IRM acquisition and hysteresis loop experiments on oriented cores showed that all samples saturate and the loops close at fields generally well below 200 mT, while generally low coercivities (B_c=4-24 mT) are observed in the samples, supporting magnetite as carrier (Fig. 2a). The thermomagnetic curves are measured in air up to 700°C that include heating and cooling cycles to check the occurrence of chemical alteration. The applied field varied from 100/180-300 mT. All sets display similar and fully reversible heating/cooling curves up to 600°C indicating that the magnetic minerals are chemically stable up to the Curie temperature of magnetite. Only upon heating to 700°C some oxidation occurs resulting in a slightly lower final cooling curve. For all basalts (TA) and mud-bricks (HM, KN, TT and the majority of TA), the highest T_c is at ~580°C pointing to magnetite as the main magnetic carrier. A small number of mud-bricks from the palace pavements (TA14-TA18) on the other hand, have a Curie temperature varying from ~500 to 580°C which indicates the presence of some low-Ti titanomagnetite. The samples from the ash layer (TA3) have a slightly higher T_c

of ~600°C which points to some cation deficient magnetite. In some of the curves from the mud-bricks and the ash layer, the heating curves display a second inflexion in the range 350-420°C, which can be interpreted as Ti-rich titanomagnetite as a second carrier. The clay furnace from Hacımusalar (HM2) and the clay pot from Tell Atchana (TA5) showed rock magnetic properties identical to the mud-bricks from the sites. Therefore, they are not displayed in figure 2a; instead they are grouped with the other mud-bricks hereafter.

For all samples, after removal of the paramagnetic contribution, we determined the ratios of remanent saturation magnetisation to saturation magnetisation M_{rs}/M_s, and the remanent coercive force to coercive force H_{cr}/H_c and plotted them in a Day plot (Day et al., 1977) as modified by Dunlop (2002) (Fig. 2b, Table S2) even though such a diagram may not sufficiently resolve the domain state of the magnetic particles (Roberts et al., 2018). The majority of the potsherds and mud-bricks are in the PSD part of the Day plot but above the SD-MD mixing lines with the exception of seven TA-P and one KIT-P potsherd that plot outside the PSD (and MD) field. The hysteresis ratios from MA-P and KIT-P potsherds plot within the distribution of the TA-P samples but their distribution is slightly more to the right (higher H_{cr}/H_c ratios) implying that these sherds are very similar to the somewhat coarser magnetic minerals of the TA-P distribution. Mud-bricks from KN and TT and the basalt samples from TA produced similar hysteresis ratios plotting in the PSD area but towards the SD field of the plot, implying generally finer-grained magnetic materials. For further (palaeointensity) analyses we discarded eight potsherds with non PSD/SD assemblage and one potsherd with an irreversible Curie curve (almost zero intensity final cooling curve due to inversion of maghemite to hematite at ~350°C).

A FORC diagram is also useful to assess the domain state of magnetic minerals and the local interaction fields for an assemblage of magnetic particles. It provides an additional check on the reliability of the hysteresis parameters such as the M_{rs}/M_s ratio which can be altered by a mixture of domain assemblages (Roberts et al., 2000). Out of 35 measurements, one representative sample from each set is shown in figure 2a. All B_c results are in

agreement with what is derived from the hysteresis experiments. The mud-brick sets KN, TA and TT have two closed inner contours with peaks at ~10 mT with narrow vertical spreading of the contours indicating that the assemblages are dominated by non-interacting PSD grains. The basalt samples have a peak at B_c=25 mT with four closed inner contours where, except for the outermost contour, all the inner contours have narrow spreading along the B_u axis which is typical for PSD grains. The ash layer from TA exhibits a distribution with a peak centered about the origin.

The low field bulk magnetic susceptibility values range between 1.55×10^{-5} to 4.02×10^{-2} SI, the majority (96%) being higher than 1.00×10^{-3} SI. The results are used to calculate the Koenigsberger ratio, Q_n, which is defined as the ratio of remanent to induced magnetisation that indicates a rocks capability to carry a stable remanence, in this case the TRM. All types of materials including the minor amount of low susceptibility samples have Q_n>1, indicating that the samples have a stable TRM (Fig. S8).

4. Archaeomagnetic Direction Determination

4.1. Demagnetisation

The analysis of the Natural Remanent Magnetisation (NRM) directions, all statistics and field tests were done through the on-line portal Paleomagnetism.org (Koymans et al., 2016). The portal uses orthogonal projection diagrams, eigenvector analysis and Fisher (1953) means. The acceptance limit of maximum angular deviation (MAD) of individual directions is taken as 10° although was typically MAD<2°, while only means with k>50 are accepted (Table 2a, Figs. 3a and 4). We regard the results as a characteristic remanent magnetisation (ChRM). We also use a test for a common true mean direction based on the coordinate bootstrap test of Tauxe (2010) which randomly samples two distributions of directions and converts those to Cartesian coordinate (x, y, z) distributions. The test is positive if all three Cartesian distributions overlap at the 95% level.

For the directional analysis, sets of 7 to 20 samples from each site are demagnetised by both thermal (2G Enterprises DC-SQUID cryogenic magnetometer) and alternating field (high precision robotized DC-SQUID magnetometer) techniques with incremental steps of 50°C up to 580-600°C or 2-5 mT up to 100 mT.

One representative demagnetisation diagram from each type of building material along with the decay curves are plotted in Figure 3a. For all sets, the viscous component is removed at low temperatures (~180-210°C) or coercivities (~10 mT). The remanence is nearly completely removed at ~580°C or 100 mT and usually decays straight to the origin. These findings from the demagnetisation diagrams and intensity decay curves are coherent with the general findings from the rock magnetic experiments, although the inflexion observed in the Curie curves from the ash layer (TA3) is not seen in the demagnetisation decay curves. Occasionally, for some sister specimens from the bottom part of the oriented core, we took the component that was heated to a sufficiently high temperature. For example, TA2.13B was clearly only heated up to 500-525°C by the destruction fire, but up to that temperature giving a component that was identical to the highest temperature component of other samples from the same site (Fig. 3a). Thermal and AF demagnetisations produced identical directions as shown by the positive coordinate bootstrap test of Tauxe (2010) (Fig. 3b). All ChRM results per site are corrected for the International Geomagnetic Reference Field (IGRF) declination at the position and time of sampling and are shown in Figure 4.

4.2. Directional Results

Hacımusalar Höyük. The demagnetisation diagrams of all sets display a stable NRM decaying to the origin. Two out of three sets (HM2 and HM3) produced acceptable results with k=104 and k=65, respectively. The relatively low k value of HM3 could be related to slight displacement of the bricks due to the thick earth cover on the top (as seen in figure S2). The demagnetisation diagrams of the third set (HM1) are also single component but

have completely random directions; hence, the collapse must have taken place after the fire event. HM1 is thus excluded from further directional analysis.

Kinet Höyük. The samples from KN1 that is composed of mud-bricks (the wall) and serpentinites (the foundation part) produced well clustered single component demagnetisation diagrams with uniform decay curves from its mud-bricks and random directions from the serpentinites. As was observed earlier by Ertepinar et al. (2016), the foundation part of the structure generally does not burn to a sufficiently high temperature to record the field. Therefore, the seven serpentinite samples are discarded, making the set of nine mud-bricks very well clustered with k=862. The samples from KN2 that is composed solely of mud-bricks also have single component demagnetisation diagrams decaying to the origin, supporting the general findings from the Curie curves. The set has a well-defined ChRM (k=366).

Tell Atchana. The sets from the site form the bulk of the directional results. Nine sets were measured for both declination and inclination and an additional five sets (repairment levels of palace pavements) were analysed for inclination only.

All mud-brick samples display an ideal magnetite magnetisation decaying straight to the origin with uniform decay curves as was also deduced from the Curie experiments (Fig. 2a). Out of five sets that are composed solely of mud-bricks, four sets (TA1, TA5, TA8, and TA9) have a well-defined ChRM direction with high k values. One mud-brick set (TA10) turned out to be not sufficiently burnt and shows random directions and is therefore excluded from further directional analysis.

The samples from the ash layer (TA3) were extremely fragile and were demagnetised only using the AF method. The NRM of the samples decay uniformly, however the remanence is not fully removed at 100 mT pointing to the presence of maghemite, which is coherent with the Curie measurements. The set has a lower k value (k=55) compared to the other sets.

This higher scatter is likely related to the fragile nature of the furnace material that makes it difficult to orient the sample.

The basalt sets (TA4 and TA19) also have single component demagnetisation diagrams where the viscous component is removed at slightly higher temperatures (~250°C). The remanence is nearly completely removed at 580°C but not yet at 100 mT, which could indicate the presence of a stable single-domain (SD) magnetite or a minor amount of maghemite (which was not observed in the Curie curves). The sets produced a well-defined ChRM with *k* values of 294 and 223, respectively.

One set that is composed of both mud-bricks and basalts (TA2) also show an extremely good cluster (*k*=979) where the directions of basalts and mud-bricks are in excellent agreement. This provides additional evidence that these mud-bricks are not strongly anisotropic.

The results of the 5 palace pavement mud-brick sets (TA14-18) are inconclusive. The high temperature/coercivity components produced 'shotgun pattern' distributions (Fig. 4). When the sets are analysed for the low temperature/coercivity component (20-150°C or 0-10 mT), there appears to be a poorly constrained cluster. When only the thermal demagnetisation results are used, there is a better cluster (with a steep inclination of 73°) but still not good enough (k=21) to give a reliable result, even though we used the 45° cut-off in Paleomagnetism.org (Fig. 4). It is likely that the palace pavement mud-bricks were baked during manufacture and as this is likely to be at a lower temperature than the destruction fires, this could result in the NRM being less stable and more prone to acquiring an overprint. Alternatively the bricks might have been randomly oriented during manufacture. Finally it is possible that the samples were not baked and instead retain a sun-dried NRM (Games, 1977). These sets are discarded from further directional analyses.

Tell Tayinat. The mud-brick samples from the single set (TT1) from the site display single component magnetite demagnetisation diagrams with a minor overprint that is removed at

210°C. The uniform decay curves and the removal of magnetisation at ~580°C are coherent with what is observed in the Curie curves. The set has a well clustered distribution (*k*=570).

In summary, out of 21 sets of samples collected from four different archaeological sites with a wide age interval of ~2000 years, 13 sets (at least one set from each site) were considered to be of sufficient good quality. Declinations range between 344.9° and 10.2° and inclinations between 36.0° and 62.9°.

5. Archaeointensity Determination

5.1. Archaeointensity Methods

Microwave experiments on potsherds. The 14GHz Tristan microwave system was used to conduct intensity experiments on all potsherd samples. The microwave frequency was individually tuned to optimise the absorption of each sample. Demagnetisation experiments were first conducted on each sherd prior to the intensity measurements to further determine the suitability of the sherd for intensity experiments (Fig. 3a). In total, 161 samples exhibited a single component decaying to the origin and were deemed suitable for archaeointensity experiments and 23 samples deemed unsuitable following the microwave demagnetisation and rock magnetic experiments. The majority of the unsuitable samples were rejected because they did not show a stable component of remanence decaying towards the origin. This is likely to have been caused by insufficient heating or by pot movement during firing.

For each selected potsherd, a subsample was subjected to a full microwave demagnetisation/remagnetisation experiment with a field applied parallel to the NRM. We followed either the Coe protocol (1967) or an IZZI protocol (Tauxe and Staudigel, 2004; Yu et al., 2004) (Fig. 5) with applied laboratory fields between 53 and 90 μT. As the KIT-P set was so small, all six samples were subject to both methods. Repeat partial microwave induced Thermoremanent Magnetisation (pT_MRM) checks were carried out to monitor possible alteration and repeat zero field checks were made as an additional alteration check and also

to detect Multi-Domain (MD) sensitivity when following the Coe protocol (Riisager and Riisager, 2001). It is recognised that applying the field parallel to the NRM direction will mask MD behaviour (Yu and Dunlop, 2003). The applied cooling rate (CR) correction protocol on potsherds is described in the Supplementary Material.

Thermal experiments on palace pavement mud-bricks. The samples from the mud-brick palace pavements of Tell Atchana (TA14-TA18) were grouped into two as University of Liverpool and Utrecht University sets.

The Liverpool experiments followed the IZZI protocol with an applied laboratory field of 53 μT, either sub-parallel or anti-parallel with additional alteration checks. Up to fourteen double heating steps were applied between 100°C and 525°C with pTRM checks after every second step.

The Utrecht set is measured with an applied laboratory field of 50 μT in a temperature range of 20-420°C. The experiments involved seven double heating steps and were performed using the IZZI protocol with the applied field randomly oriented with respect to the NRM of the sample. The measurements were carried out with one pTRM check, enabled after the final double heating step of the experiment (Fig. 5). The CR corrections on pavement bricks are described in the Supplementary Material and show that CR effects are minimal.

Combined microwave and thermal experiments on oriented mud-bricks. Mainly thermal (Utrecht) and a minor amount of microwave (Liverpool) experiments were run on six sets of mud-brick samples either following IZZI or Coe protocol with applied fields between 40 and 100 μT. Microwave experiments were carried out with the applied field parallel or anti-parallel to the NRM of the samples, whereas thermal experiments were performed using a custom built orientation tray that enables aligning samples individually to desired angles, in this case parallel to the NRM. In the microwave experiments, pTRM checks were performed after every double treatment to monitor the possible influence of alteration. Thermal experiments

were carried out with pTRM checks either fully enabled in every two double heating steps or one successful check at the end of the experiment (Fig. 5).

Due to the lengthy nature of CR experiments we did not investigate the effect of cooling on these data sets, however, based on earlier results (Biggin et al., 2013; Yu, 2011), our previous experiments on the PSD mud-bricks (Ertepinar et al., 2012), our results on the Tell Atchana pavement mud-bricks from this study and the consistency between microwave and thermal experiments which have very different cooling times suggest the CR effects are minimal and hence can be neglected.

5.2. Anisotropy Determination

Pottery has been shown to be strongly anisotropic (Chauvin et al., 2000) due to the preferential alignment of magnetic grains presumed to be induced during the creation of the ceramic artefact. For both wheel and hand-made pottery, if the clay is worked into a particular orientation it is probable that the plate-like clay particles become aligned during fabrication and cause a similar alignment of the magnetic minerals (Yang et al., 1993) that can lead to an error in the intensity estimation of up to 50% (Gómez-Paccard et al., 2019). In order to mitigate the effects of anisotropy, the field was applied parallel to the NRM direction (Rogers et al., 1979). The effectiveness of this method is further confirmed by Odah et al. (2001) who determined accurate palaeointensities from experimentally manufactured ceramics. As an additional check, the angle γ between the pTRM acquired at the last step used for the best-fit segment and the applied field direction (Biggin and Paterson, 2014) was checked for all potsherds and also the mud-bricks.

5.3. Selection criteria

For both microwave and thermal experiments, following criteria are followed:

1. The number of points (N) defining the slope: N≥5

2. The ratio of standard error of the slope to absolute value of the slope β<0.1 (Selkin and Tauxe, 2000)
3. The lower acceptance limit for the NRM fraction: f≥0.35 (Coe et al., 1978). However, except for two measurements, f values are much higher
4. The acceptance criterion of quality factor (q) is 3
5. The upper acceptance limits for the angle between anchored and non-anchored best-fit vector (α) (Selkin and Tauxe, 2000) is taken as 10°
6. MD behaviour of the interpreted segment of the NRM-TRM plot is assessed by the curvature statistics, $|k'|$, and the acceptance limit is taken as 0.164 as suggested by Paterson (2011), but we accepted two sherds with $|k'|$=0.169
7. pTRM checks (where applicable) were deemed to have been successful if the ratio of the difference between the check and the relevant TRM value to the length of the selected NRM-TRM segment (DRAT) was smaller than 10% (Selkin and Tauxe, 2000) and the cumulative DRAT (CDRAT), defined as the sum of all the DRATs, should be less than 11% (Paterson et al., 2014)

5.4 Archaeointensity Results

Potsherds. Archaeointensity experiments on potsherds were carried out on 114 individual sherds from Tell Atchana (TA-P), 6 from Kilise Tepe (KT-P), 5 from Bellapais Vounous (BV-P) and 22 from Marki Alonia (MA-P). We did experiments on an additional 14 sister samples (Table S3a).

From TA-P, 56 out of 114 individual potsherds (57 measurements) passed all the criteria yielding a success rate of 49%. The values for the angle γ is found to be <5° for the majority (forty-five) of the potsherds, eight have 5°<γ<10° and the remaining four have γ>10°. On average, the CR correction factor was 0.85 with the largest correction factor being 0.73 for Level IV. An unusual positive correction factor of 1.08 was recorded for Level XVII/XVIII. For the majority of levels it was only possible to carry out one CR correction experiment. The site

mean (CR corrected) intensity values from the potsherds of TA-P range from 39.8 to 55.1 μT. Over the duration of the occupation of the site (2200-1300 BC) the field fluctuated between this maximum and minimum. The highest field value of 55.1 μT was recorded for the lowermost level (Level XVII/XVIII) which represents the earliest occupation level of the site, ~2200-2000 BC, whereas the lowest value was from Level IX (1675-1575 BC) (Table 2b).

The results from KIT-P have a much lower success rate (38%) on specimen basis, where one to two sister specimens from each sherd failed to meet the acceptance criteria. The set with the largest age interval (level I/II) did not provide any successful result from two measurements on the single sherd from the level. Two sets, levels IIa and IId, produced one successful result each, where both measurements are of good quality with similar (and high) intensity values of 83.2 and 84.1 μT, respectively. Unfortunately, no samples from these sets survived for the CR experiments. The fourth set (level IIe) again did not provide any result from the single sherd. The final set, level IIf (800-650 BC), produced a CR corrected mean intensity value of 81.9 μT from three successful measurements performed on two sherds. Individual CR measurements on these sherds are found to be 0.84 and 0.82. The angle γ for the successful measurements is found to be 3.4° on average (highest being 6.3°).

Out of a sample set of 27 Cypriot sherds, 14 gave acceptable results, (success rate of 52%). The site MA-P had the largest variety of pottery typology among all sites. It is noted that there is no apparent pattern in the samples that were unsuccessful/successful which could be related to pottery type. The first group of samples consisting of Red Polished Ware, Red Polished Coarse Ware and Drab Polished Ware produced a CR corrected archaeointensity value of 38.8 μT from five potsherds out of thirteen. The second set was composed of only one Red Polished Ware sherd from Early Cypriot I-II where the CR corrected intensity value is 53.0 μT from a single measurement. The oldest set with Red Polished Philia Ware yielded four acceptable results out of nine with a mean CR corrected intensity value of 53.8 μT. The experiments run on the potsherds from BV-P produced a CR corrected mean intensity value of 46.4 μT from four potsherds out of five. The correction factor of 0.83 was adapted from the

same pottery type of MA-P (Red Polished Ware) since all potsherds showed sign of alteration (Table S3a). The angle γ is <6.6° for the accepted Cypriot potsherds (2.6° on average). In all cases, the intensity determined was consistent with the other results for the level (Table S3). We therefore conclude that anisotropy is not biasing our results.

For some potsherd levels there is a significant range in intensity values. For example, TA-P Level II/III has a range of 15.7 μT, while Level XVII/XVIII has 21.5 μT and MA-P Early Cypriot II/Middle Cypriot I level has 24.4 μT. Correspondingly, the standard deviations are high even though in some cases one single value determines the large range. For example, if we disregard the 43.2 result in the TA-P Level II/III the range becomes 3.5 μT.

Mud-bricks. Of all 66 mud-brick samples only 18 failed, implying a high success rate of 73%. Of the 18 failed samples, 12 failed for a combination of criteria, but 6 failed due to the curvature parameter only.

The mud-brick samples from the palace pavements (TA14-TA18) gave no useful directional data, but gave consistent archaeointensity results with very little zigzagging in the NRM-TRM plots. This suggests that the mud-bricks were manufactured in random orientations rather than having an unstable NRM or being sun-dried. The sets have a very high success rate of 85%. For the youngest (TA14) and oldest (TA15) levels we did not perform the CR experiment. However, from the three sets where we did establish a CR factor for each set, the intensities were 1.3-2.4 μT lower, well within the standard deviation. Hence, CR effects are minimal for this data set, in line with our earlier conclusions (Ertepinar et al., 2016). The highest and lowest mean intensity recorded are 45.2 and 37.7 μT (Table 2b, Table S3b).

Out of six sets of mud-bricks -which all gave good directional results- five sets gave acceptable archaeointensity results from at least two samples per set, only one set (TA5) failed. For all the accepted results, the angle γ is found to be <5.3°, suggesting that the anisotropy effects are minimal. The highest success rates of 83.3% and 67% are from TA

Level 4 and Level 7 Palace samples, respectively. The mean intensity values for the sets are 67.2 and 65.9 μT.

The single set from Tell Tayinat (TT1, ~672 BC) produced two successful thermal results (out of four) with a mean intensity value of 96.7±2.1 μT. The fifth measurement (microwave) yielded an unrealistic overshoot result (482.5 μT) which failed in the curvature parameter, |k'|.

The two remaining passed sets are from Kinet Höyük (KN1 and KN2). Samples from KN1 had an indestructible NRM and therefore the NRM fraction (f) remained much lower than the acceptance limits even when high powers were applied, that caused a melting spot indicating alteration. The success rate for the level is 25% (6 rejections out of 8). The two successful results (one TT and one MW) are in good agreement with each other with a mean intensity value of 55.2±0.9 μT. Thermal measurements on two samples from KN2 gave a mean intensity value of 64.9±1.2 μT (Table 2b).

6. Discussion

6.1 Directions

The majority of the directional data presented in this study (Figs. 6a and b) are from an age interval (mostly 1875-1465 BC) and region that is lacking data. The new results, following the IGRF correction for the declinations, are plotted against the data from Geomagia50.v3.2 (downloaded on December 2018) (Brown et al., 2015), the data from Turkey, Cyprus and Israel (Ertepinar et al., 2016, 2012; Shaar et al., 2016; Tema et al., 2018) and the global field model SHA.DIF.14k (Pavon-Carrasco et al., 2014). The data are relocated to and the models are calculated at Kayseri (38.85°N, 35.63°E), the approximate center of Turkey.

The declinations from the youngest data set TT1 is more to the west (D=350.2±4.2) compared to the predictions of the model SHA.DIF.14k, although it just overlaps within error the westward swing seen in the model, but the direction is in excellent agreement with the

484 near contemporaneous data point (D=349.5±8.5) from (Ertepinar et al., 2012). These two
485 data points, which are well constrained in age, confirm the existence of a westerly swing
486 suggested to have occurred between 780-690 BC by SHA.DIF.14k. The inclination value of
487 the site (I=62.7±2.7) is slightly shallower than predictions of SHA.DIF.14k (~4.5°), but again
488 in excellent agreement with the Ertepinar et al. (2012) inclination (I=61.8±5.5).

489 There are ten data points from 1650-1465 BC (all TA sets, KN2 and HM3) that show a trend
490 from east (~10°) to west (~-15°), towards younger ages, with the exception of one single data
491 point (TA5). The declination curve from SHA.DIF.14k has a very similar trend from 1800 to
492 1450 BC in approximately the same age interval, from ~7° east to ~5° west, and the model is
493 coherent with the trend of our new data points. However, the westernmost and easternmost
494 declination values of our data are exaggerated by some 5-10° compared to the model curve
495 which is likely due to the inherent smoothing in constructing the model. The reason for the
496 misfit declination of TA5 is likely related to our (apparently unsuccessful) attempt to restore
497 the directions of the *ex-situ* hearth to its original position relying on the grid plans (Fig. S5b).
498 For the age interval of our data points, SHA.DIF.14k predicts a continuous increase in the
499 inclination where our data are in good agreement with this increasing trend. Data points TA2,
500 TA4 and TA19 would fit better with the model when plotted on the younger end of their age
501 uncertainty. This could be a reasonable interpretation considering all three sets are from the
502 same heavily burnt destruction level which ended the Level VII era. The trend in inclination is
503 in excellent agreement with a similar trend in inclination from Ertepinar et al. (2016). Also our
504 inclinations are exaggerated, by some 10°, because of model smoothing.

505 The direction from KN1 plots perfectly in line with the Ertepinar et al. (2016) data, both in
506 declination and inclination, slightly to the west of SHA.DIF.14k predictions. The inclination
507 value of the set is 10-15° shallower than the model predictions but in good agreement with
508 Geomagia50.v3.2 data within a few degrees.

The oldest data point HM2, displays a direction consistent with the model, but this is largely due to the large errors in declination and inclination, while the site also has an extremely large age uncertainty of ±600 years.

We then compared our new directional data to the best available PSV curves in the region, Greece (De Marco et al., 2014) and Bulgaria (Kovacheva et al., 2014), without their published error bounds for better readability (insets in Figs. 6a and b). Clearly, our youngest data (TT1) around 700 BC excellently fit the Greek curve both in declination and inclination. Between 1600 and 1300 BC there is poor to reasonable correspondence; the declination swing in our data (TA1, TA8 and TA9) is not seen in either curve, but our inclinations fit both curves reasonably well. Also our earlier swing to western declination between 2000 and 1700 BC (Ertepinar et al., 2016) is not seen in either curve, but the conspicuous swing to shallower inclinations in the Turkish data is excellently covered in the Greek curve, but not in the Bulgarian curve.

Out of the 13 sites with directional information we have the palaeointensity for 5 sites, thus providing the full field vector (Table 3).

6.2 Archaeointensities

The geomagnetic field in the Middle East over the time period from 3000-0 BC is marked by at least one period of extremely high field intensity, the LIAA (Shaar et al., 2017, 2016) dated to between 1050 and 700 BC. Shaar et al. (2017) argue that it actually consists of two spikes, with VADMs up to 180 ZAm^2, with slightly lower VADMs<140 ZAm^2 between the spikes. This high intensity was also confirmed in Turkey (Arslantepe, 176 ZAm^2, Ertepinar et al., 2012). The geographic extent of the LIAA and the exact duration of these spikes remain unclear. Recently, Shaar et al. (2016) suggested these spikes are caused by a regional anomaly which extends further to the east (Georgia, 45°E), but has a limited extension to the west, at about 30-35°E. This is mainly based on the argument of Shaar et al. (2017) that there is no evidence for the LIAA in Greece and Bulgaria. However, it is evident that there

535 are very few data in Bulgaria in the LIAA age interval, although the slightly larger database
536 for Greece does not show intensities >105 ZAm^2 either. The LIAA may extend further east, to
537 Turkmenistan at 60-65°E where intensities >145 ZAm^2 are found. In their study of Holocene
538 lavas from the Canary Islands, de Groot et al. (2015) find high palaeointensities ~120 ZAm^2
539 at 826-723 BC. Recently, Béguin et al. (2019) used three marine sediment cores from the
540 Mediterranean to better constrain the LIAA in time and space. They suggested that the LIAA
541 moves from 40 to 55° East at 1000 BC to ~25° East at 0 CE, while decaying from ~150 to
542 ~110 ZAm^2 in the same time span. This is partly based on the relatively low palaeointensities
543 they find in their westernmost core in the Alboran Sea (<80 ZAm^2). However, in Portugal
544 Nachasova and Burakov (2009) find palaeointensities higher than 140 ZAm^2 in the LIAA
545 interval (880-730 BC) and higher than 160 ZAm^2 around 500 BC, while a recent study of
546 Molina-Cardín et al. (2018) reports the highest intensities ever recorded in Spain, ranging
547 144-152 ZAm^2 around 600 BC. Earlier, Hervé et al. (2013) found high intensities for Western
548 Europe (relocated at Paris) of more than 140 ZAm^2 around 800 BC. Interestingly, Bourne et
549 al. (2016) find high relative palaeointensities from a cave deposit in Texas for the similar time
550 interval (modelled at 893±135 BC). They suggest an almost four-fold increase in
551 geomagnetic field intensity lasting several hundred years and presents evidence for the
552 existence of an intensity high in North America that is roughly contemporaneous with the
553 similar duration of the LIAA, although the age of the (single) spike is between the two spikes
554 at ~980 and ~740 BC. They argue that the cave record may provide evidence for flux lobes
555 as seen in the present-day field, and effects of the Near East lobe is mirrored by the North
556 American lobe. Clearly, the nature of the LIAA in space and time, as a regional or global
557 feature is still far from resolved.

558 This study presents thirty-one new sets of archaeointensity results, two of which are from a
559 period of suggested high intensities. Out of thirty-one, three sets of potsherds gave only one
560 successful result. Even though N=1 cannot by any means be considered reliable, the results
561 from these sets are still reported (Table 2b), but displayed separately from the rest of the

group (Fig. 6c). The remaining sets have successful measurements (N ranging 2 to 9). The VADM of the sets are plotted against the field model SHA.DIF.14k, the data from the Middle East, Cyprus, Georgia, Turkey (mostly our own compilation from the respective papers) and Geomagia50.v3.2 data.

The oldest four results are from the Cypriot potsherds from an age interval of 2325-2000 BC, where BV-P produced a mean which is spot on the SHA.DIF.14k prediction; all sets, ranging 71-99 ZAm^2, are coherent with the Middle East data and within error fit the model predictions. The set with a single successful measurement (97.0 ZAm^2) is also in agreement with the Middle East data but here we have no standard deviation.

The dataset from Tell Atchana potsherds provides the first semi-continuous archaeointensity sequence from a single location in Turkey spanning the age interval 2100-1350 BC. All fourteen data points differ from SHA.DIF.14k by at most 10 ZAm^2, with the means ranging 71.9-99.4 ZAm^2. In general, the means are within error of the SHA.DIF.14k model, and nicely follow its trend for this age interval.

The five sets from Kilise Tepe gave rather disappointing results. Two sets produced no results, another two sets provided no acceptable results because of only one successful measurement. Only one set produced an acceptable result. The N=1 results from 1300 and 1150 BC (plotted dark green and transparent in Fig. 6c) are significantly higher than both models (by at least 40 ZAm^2) and much higher than the Middle East and Geomagia50.v3.2 data. The successful set consisting of three measurements has a VADM of 147±11 ZAm^2 at 725±75 BC. This result is higher than both models but in agreement with the Middle East and Georgia data and confirms the existence of the younger spike of the LIAA suggested by Shaar et al. (2017). It should be noted that even the rejected measurements from the set are consistently high, ranging 140-160 ZAm^2 (Table S3a).

Mud-brick sets from the repairment levels of palace pavements TA14-TA18 that have the highest success rate display a continuous steady decrease in the intensity from 81.6 to 68.1

588 ZAm^2 for the age interval between 2040 and 1675 BC, contemporaneous with the oldest ten
589 sherd levels from Tell Atchana. There are no systematic differences observed for the
590 potsherds and mud-bricks results. The decrease in the intensity is extended to younger ages
591 by some 150 years compared to SHA.DIF.14k. This trend is followed by an abrupt increase
592 to 79.1 ZAm^2 within some 50 years. The other two mud-brick sets from TA (Levels IV and VII
593 at 1465 and 1625 BC) are both much higher (~120 ZAm^2) than the model predictions that
594 range 80-100 Zam^2 during this time span. Only the younger data point is consistent with
595 some of the data from Geomagia50.v3.2.

596 From Kinet Höyük we have two acceptable intensity results of 98.8 ZAm^2 (KN1 at 1875 BC)
597 and 116.1 ZAm^2 (KN2 at 1650 BC). The intensity of KN1 -although higher than SHA.DIF.14k-
598 is in excellent agreement with the high intensities ranging 90-106 ZAm^2 found during this
599 time by Ertepinar et al. (2016). The intensity of KN2 is similar to that of TA Level VII (118.9
600 Zam^2) at 1625 BC (Fig. 6c). When compared to the two potsherd results from the same age,
601 there is a significant difference, the potsherds having lower intensities by ~45 ZAm^2, almost
602 40%. The cooling rate effect cannot explain this discrepancy, since the mean effect in our
603 mud-bricks is on average 5%, in line with the majority of the estimates (mostly 4-10%) from
604 the compilation of (Genevey et al., 2008). The older set KN1 has one microwave and one
605 thermal measurement which are extremely consistent (Table S3b) despite the very different
606 cooling times of a few seconds (MW) to up to an hour (TT). The VADM plot shows that the
607 potsherd results are more consistent with Geomagia50.v3.2 data and the SHA.DIF.14k
608 predictions. Since there is no clear preference in terms of data quality, we cannot favour any
609 of the two results over the other two. Although very rapid changes have been shown to occur
610 (e.g. during the LIAA), we lack sufficient data to speculate on this.

611 The set from Tell Tayinat (TT1) from ~672 BC has a very high intensity of 174.4 ZAm^2, and
612 equals the highest VADMs found by Shaar et al. (2016). This confirms the LIAA younger
613 spike to be recorded in Turkey.

Finally, we applied a number of strict criteria on Geomagia50.v3.2 data, following Poletti et al. (2018). However, we were more lenient on the age error (±250 year instead of ±100) and we did not require MD monitoring. These criteria removed about 80% of the Geomagia50.v3.2 data (inset in Fig. 6c). The major improvement applying the strict criteria is on the age interval of 2300-1300 BC, where there is significantly less scatter. Our contribution from this study doubles the available data for this time interval.

7. Conclusions

In this study, we present thirteen new directional data five of which provide the full vector of the field. The recorded directions show larger swings than the models for both declination and inclination, which we contribute to the inherent smoothing in the construction of the models. This was also noted earlier by Ertepinar et al. (2016) who found similar larger directional swings than the models. Hence, our earlier and present data contribute significantly to improving the resolution of existing models, in particular for this region.

In addition, we provide thirty-one new archaeointensity results from both potsherds and mud-bricks. The potsherds from Tell Atchana provide the longest sequence from 2100 to 1350 BC recorded so far in Turkey. In general, the results agree well with existing data from the Middle East, and are usually in reasonable agreement with model predictions. Applying strict criteria (Poletti et al., 2018) on Geomagia50.v3.2 archaeointensity data improves the resolution for the age interval of 2300-1300 BC and the data presented in this study doubles the amount of high-quality data for this time interval. The conspicuous high intensity interval of the LIAA is further confirmed in Turkey; in particular the younger spike of the LIAA is recorded by our new data, both in well-dated mud-bricks and potsherds, from two different locations (Tell Tayinat and Kilise Tepe). Earlier, we provided evidence for very high intensities in the older spike of the LIAA as recorded in Arslantepe by Ertepinar et al. (2012). It appears that the LIAA is a robust feature, at least in the Levant and Middle East. Its spatial and temporal extents, however, require more records from geographically distinct areas.

Acknowledgements

We are grateful to Nicholas Postgate and Mara Horowitz for engaging in fruitful discussions. Nicholas Postgate is also thanked for supplying the samples from Kilise Tepe. We are grateful to Ben Claasz Coockson and people in the excavation teams who were helpful at all times. We thank Nuretdin Kaymakci -the drilling expert- who has been a great help in the field. MLH acknowledges a Natural Environment Research Council studentship held at the University of Liverpool. MJH acknowledges NERC grant NE/I013873/1. The editor and two reviewers are thanked for their thorough reviews.

Figure Captions

Figure 1. Location map of studied sites from the Mediterranean (red). Green circles are the previously published data from Anatolia and Upper Mesopotamia, Turkey. Blue circles are the data from the Middle East (see the text for references).

Figure 2. (a) Representative Curie curves, hysteresis loops (displayed after the paramagnetic correction on a mass-specific basis), IRM acquisition curves of potsherds and oriented cores from each sampling site. For all potsherds, the Curie curves are almost fully reversible, where red (blue) lines are the heating (cooling) curves, with T_c at ~580°C indicating the presence of magnetite as the main carrier. The inflexion at ~300°C in KIT-P sample points the presence of Ti-rich titanomagnetite. Samples from BV-P exhibit a paramagnetic contribution in their Curie curves and hysteresis loops. IRM acquisition curves (green lines) for all samples show saturations fields of well below 300 mT. All oriented cores display near reversible heating (red) and cooling (blue) curves, with T_c at ~580°C indicating the presence of magnetite. A second inflexion at 350-420°C observed in ash layer of TA and mud-brick of TT can be interpreted as Ti-rich titanomagnetite as a second carrier. IRM acquisition curves (green lines) for all samples show saturations fields <200 mT. The FORC diagrams of oriented cores are generated using a smoothing factor (SF) of 3 and contour interval of 10. All mud-brick and basalt samples have closed inner contours and display narrow vertical spreading indicating the dominance of non-interacting PSD grains. (b) Hysteresis ratios plotted in Day plot modified by Dunlop (2002). Majority of the samples plot above the SD-MD mixing lines but well into the PSD field of the plot.

Figure 3. (a) Stepwise microwave - MW (potsherds), and thermal-Th or alternating field-AF (oriented samples) demagnetisation diagrams. Closed (open) symbols represent the projection of the vector end-points on the horizontal (vertical) plane; values represent microwave power/time in Watt/second, temperature in °C or alternating field in or mT. Normalized intensity decay plots are also shown for the oriented samples. All samples,

except for a partially burnt mud-brick from TA where there is a low-temperature (LT) and a high temperature (HT) component, display a single component demagnetisation diagram decaying to the origin. (b) Comparison of Th and AF demagnetisations using the coordinate bootstrap test (Tauxe, 2010) for randomly selected mud-brick set (KN2).

Figure 4. The characteristic remanent magnetisation (ChRM) directions. The red circles are α_{95} cone of confidence, k is dispersion parameter and D/I is the declination and inclination. For the inclination only sets (TA14-TA18), high-temperature/high coercivity (HT/HC) and low-temperature/low coercivity (LT/LC) components are shown separately.

Figure 5. NRM-TRM plots of one representative example from each sample set and associated orthogonal vector plots in core coordinates. The arrows represent the $pT_{(M)}RM$ checks and the squares are pT_MRM tail checks enabled when applying the Coe protocol on potsherds. Closed (open) circles are accepted (rejected) double heating steps; values represent microwave power/time in Watt/second or temperature in °C. Solid blue (open green) circles on the orthogonal plots are horizontal (vertical) planes and the plots are single component decaying towards the origin.

Figure 6. New (a) declination and (b) inclination data (red) plotted against Geomagia50.v3.2 data (gray), data from Turkey (blue, pink and orange), Cyprus and Israel (green) and the global field models SHA.DIF.14k (green). The insets are data from this study and Ertepinar et al. (2016, 2012) data plotted against PSV curves from Greece and Bulgaria. (c) site mean VADMs of potsherds (red diamonds) and mud-bricks (red circles) along with the data from Geomagia50.v3.2 (gray), the Middle East, Cyprus, Georgia (orange), and Turkey (blue and pink) and the global field model SHA.DIF.14k (green). The sets with only one successful measurement (N=1) are displayed dark green and transparent. The inset shows comparison of the data from this study, Ertepinar et al. (2016, 2012) data and Geomagia50.v3.2 data with modified Poletti et al. (2018) cut-offs.

References

Béguin, A., Filippidi, A., de Lange, G.J., de Groot, L. V., 2019. The evolution of the Levantine Iron Age geomagnetic Anomaly captured in Mediterranean sediments. Earth Planet. Sci. Lett. 511, 55–66. doi:10.1016/j.epsl.2019.01.021

Ben-Yosef, E., Millman, M., Shaar, R., Tauxe, L., Lipschits, O., 2017. Six centuries of geomagnetic intensity variations recorded by royal Judean stamped jar handles. Proc. Natl. Acad. Sci. 114, 2160–2165. doi:10.1073/pnas.1615797114

Ben-Yosef, E., Ron, H., Tauxe, L., Agnon, A., Genevey, A., Levy, T.E., Avner, U., Najjar, M., 2008a. Application of copper slag in geomagnetic archaeointensity research. J. Geophys. Res. Solid Earth 113. doi:10.1029/2007JB005235

Ben-Yosef, E., Tauxe, L., Levy, T.E., Shaar, R., Ron, H., Najjar, M., 2009. Geomagnetic intensity spike recorded in high resolution slag deposit in Southern Jordan. Earth Planet. Sci. Lett. 287, 529–539. doi:10.1016/j.epsl.2009.09.001

Ben-Yosef, E., Tauxe, L., Ron, H., Agnon, A., Avner, U., Najjar, M., Levy, T.E., 2008b. A new approach for geomagnetic archaeointensity research: insights on ancient metallurgy in the Southern Levant. J. Archaeol. Sci. 35, 2863–2879. doi:10.1016/j.jas.2008.05.016

Biggin, A.J., Badejo, S., Hodgson, E., Muxworthy, A.R., Shaw, J., Dekkers, M.J., 2013. The effect of cooling rate on the intensity of thermoremanent magnetization (TRM) acquired by assemblages of pseudo-single domain, multidomain and interacting single-domain grains. Geophys. J. Int. 193, 1239–1249. doi:10.1093/gji/ggt078

Biggin, A.J., Paterson, G.A., 2014. A new set of qualitative reliability criteria to aid inferences on palaeomagnetic dipole moment variations through geological time. Front. Earth Sci. 2, 1–9. doi:10.3389/feart.2014.00024

Bourne, M.D., Feinberg, J.M., Stafford, T.W., Waters, M.R., Lundelius, E., Forman, S.L., 2016. High-intensity geomagnetic field “spike” observed at ca. 3000 cal BP in Texas, USA. Earth Planet. Sci. Lett. 442, 80–92. doi:10.1016/j.epsl.2016.02.051

Brown, M.C., Donadini, F., Korte, M., Nilsson, A., Korhonen, K., Lodge, A., Lengyel, S.N., Constable, C.G., 2015. GEOMAGIA50.v3: 1. general structure and modifications to the archeological and volcanic database. Earth, Planets Sp. 67, 83. doi:10.1186/s40623-015-0232-0

Chauvin, A., Garcia, Y., Lanos, P., Laubenheimer, F., 2000. Paleointensity of the geomagnetic field recovered on archaeomagnetic sites from France. Phys. Earth Planet. Inter. 120, 111–136. doi:10.1016/S0031-9201(00)00148-5

Coe, R.S., 1967. Paleo-intensities of the Earth’s magnetic field determined from Tertiary and Quaternary rocks. J. Geophys. Res. 72, 3247–3262. doi:10.1029/JZ072i012p03247

Coe, R.S., Grommé, S., Mankinen, E.A., 1978. Geomagnetic paleointensities from radiocarbon-dated lava flows on Hawaii and the question of the Pacific nondipole low. J. Geophys. Res. 83, 1740–1756. doi:10.1029/JB083iB04p01740

Day, R., Fuller, M., Schmidt, V.A., 1977. Hysteresis properties of titanomagnetites: Grain-size and compositional dependence. Phys. Earth Planet. Inter. 13, 260–267. doi:10.1016/0031-9201(77)90108-X

de Groot, L. V., Béguin, A., Kosters, M.E., van Rijsingen, E.M., Struijk, E.L.M., Biggin, A.J., Hurst, E.A., Langereis, C.G., Dekkers, M.J., 2015. High paleointensities for the Canary

742 Islands constrain the Levant geomagnetic high 419, 154–167.
743 doi:10.1016/j.epsl.2015.03.020

744 De Marco, E., Tema, E., Lanos, P., Kondopoulou, D., 2014. An updated catalogue of Greek
745 archaeomagnetic data for the last 4500 years and a directional secular variation curve.
746 Stud. Geophys. Geod. 58, 121–147. doi:10.1007/s11200-013-0910-y

747 Dunlop, D.J., 2002. Theory and application of the Day plot (Mrs/Ms versus Hcr/Hc) 2.
748 Application to data for rocks, sediments, and soils. J. Geophys. Res. 107.
749 doi:10.1029/2001JB000487

750 Ertepinar, P., Langereis, C.G., Biggin, A.J., de Groot, L. V., Kulakoğlu, F., Omura, S., Süel,
751 A., 2016. Full vector archaeomagnetic records from Anatolia between 2400 and 1350
752 BCE: Implications for geomagnetic field models and the dating of fires in antiquity. Earth
753 Planet. Sci. Lett. 434, 171–186. doi:10.1016/j.epsl.2015.11.015

754 Ertepinar, P., Langereis, C.G., Biggin, A.J., Frangipane, M., Matney, T., Ökse, T., Engin, A.,
755 2012. Archaeomagnetic study of five mounds from Upper Mesopotamia between 2500
756 and 700 BCE: Further evidence for an extremely strong geomagnetic field ca. 3000
757 years ago. Earth Planet. Sci. Lett. 357–358, 84–98. doi:10.1016/j.epsl.2012.08.039

758 Fisher, R.A., 1953. Dispersion on a sphere. Proc. R. Soc. London 217A, 295–305.

759 Gallet, Y., Butterlin, P., 2015. Archaeological and geomagnetic implications of new
760 archaeomagnetic intensity data from the Early Bronze high terrace 'Massif Rouge' at
761 Mari (Tell Hariri, Syria). Archaeometry 57, 263–276. doi:10.1111/arcm.12112

762 Gallet, Y., D'Andrea, M., Genevey, A., Pinnock, F., Le Goff, M., Matthiae, P., 2014.
763 Archaeomagnetism at Ebla (Tell Mardikh, Syria). New data on geomagnetic field
764 intensity variations in the Near East during the Bronze Age. J. Archaeol. Sci. 42, 295–
765 304. doi:10.1016/J.JAS.2013.11.007

766 Gallet, Y., Genevey, A., Courtillot, V., 2003. On the possible occurrence of "archaeomagnetic
767 jerks" in the geomagnetic field over the past three millennia. Earth Planet. Sci. Lett. 214,
768 237–242. doi:10.1016/S0012-821X(03)00362-5

769 Gallet, Y., Genevey, A., Le Goff, M., Fluteau, F., Ali Eshraghi, S., 2006. Possible impact of
770 the Earth's magnetic field on the history of ancient civilizations. Earth Planet. Sci. Lett.
771 246, 17–26. doi:10.1016/j.epsl.2006.04.001

772 Gallet, Y., Le Goff, M., Genevey, A., Margueron, J., Matthiae, P., 2008. Geomagnetic field
773 intensity behavior in the Middle East between ~3000 BC and ~1500 BC. Geophys. Res.
774 Lett. 35. doi:10.1029/2007GL031991

775 Gallet, Y., Molist Montaña, M., Genevey, A., Clop García, X., Thébault, E., Gómez Bach, A.,
776 Le Goff, M., Robert, B., Nachasova, I., 2015. New Late Neolithic (c. 7000–5000 BC)
777 archeointensity data from Syria. Reconstructing 9000 years of archeomagnetic field
778 intensity variations in the Middle East. Phys. Earth Planet. Inter. 238, 89–103.
779 doi:10.1016/J.PEPI.2014.11.003

780 Games, K.P., 1977. The magnitude of the palaeomagnetic field: a new non-thermal,
781 non-detrital method using Sundried bricks. Geophys. J. R. Astron. Soc. 48, 315–329.
782 doi:10.1111/j.1365-246X.1977.tb03675.x

783 Genevey, A., Gallet, Y., Constable, C.G., Korte, M., Hulot, G., 2008. ArcheoInt: An upgraded
784 compilation of geomagnetic field intensity data for the past ten millennia and its
785 application to the recovery of the past dipole moment. Geochemistry, Geophys.
786 Geosystems 9. doi:10.1029/2007GC001881

787 Genevey, A., Gallet, Y., Margueron, J.-C., 2003. Eight thousand years of geomagnetic field
788 intensity variations in the eastern Mediterranean. J. Geophys. Res. 108.
789 doi:10.1029/2001JB001612

790 Gómez-Paccard, M., Chauvin, A., Albeck, M.E., Zaburlín, M.A., Basso, D.M., Pavón-
791 Carrasco, F.J., Osete, M.L., Campuzano, S.A., 2019. New archeointensity data from
792 NW Argentina (1300–1500 CE). Phys. Earth Planet. Inter. 286, 92–100.
793 doi:10.1016/j.pepi.2018.11.004

794 Hervé, G., Chauvin, A., Lanos, P., 2013. Geomagnetic field variations in Western Europe
795 from 1500BC to 200AD. Part II: New intensity secular variation curve. Phys. Earth
796 Planet. Inter. 218, 51–65. doi:10.1016/j.pepi.2013.02.003

797 Kovacheva, M., Kostadinova-Avramova, M., Jordanova, N., Lanos, P., Boyadzhiev, Y., 2014.
798 Extended and revised archaeomagnetic database and secular variation curves from
799 Bulgaria for the last eight millennia. Phys. Earth Planet. Inter. 236, 79–94.
800 doi:10.1016/J.PEPI.2014.07.002

801 Koymans, M.R., Langereis, C.G., Pastor-Galán, D., van Hinsbergen, D.J.J., 2016.
802 Paleomagnetism.org: An online multi-platform open source environment for
803 paleomagnetic data analysis. Comput. Geosci. 93, 127–137.
804 doi:10.1016/j.cageo.2016.05.007

805 Molina-Cardín, A., Campuzano, S.A., Osete, M.L., Rivero-Montero, M., Pavón-Carrasco,
806 F.J., Palencia-Ortas, A., Martín-Hernández, F., Gómez-Paccard, M., Chauvin, A.,
807 Guerrero-Suárez, S., Pérez-Fuentes, J.C., McIntosh, G., Catanzariti, G., Sastre Blanco,
808 J.C., Larrazabal, J., Fernández Martínez, V.M., Álvarez Sanchís, J.R., Rodríguez-
809 Hernández, J., Martín Viso, I., Garcia i Rubert, D., 2018. Updated Iberian
810 Archeomagnetic Catalogue: New Full Vector Paleosecular Variation Curve for the Last
811 Three Millennia. Geochemistry, Geophys. Geosystems 19, 3637–3656.
812 doi:10.1029/2018GC007781

813 Mullender, T.A.T., van Velzen, A.J., Dekkers, M.J., 1993. Continuous drift correction and
814 separate identification of ferrimagnetic and paramagnetic contributions in
815 thermomagnetic runs. Geophys. J. Int. 114, 663–672. doi:10.1111/j.1365-
816 246X.1993.tb06995.x

817 Nachasova, I.E., Burakov, K.S., 2009. Variation of the intensity of the Earth's magnetic field
818 in Portugal in the 1st millennium BC. Izv. Phys. Solid Earth 45, 595–603.
819 doi:10.1134/s1069351309070040

820 Odah, H., Hussain, A.G., Hoffmann, V., Soffel, H.C., El-Gamili, M., Deebes, H., 2001. Effect
821 of magnetic anisotropy on the experimentally determined palaeointensity of the
822 geomagnetic field. Earth, Planets Sp. 53, 363–371. doi:10.1186/BF03352393

823 Paterson, G.A., 2011. A simple test for the presence of multidomain behavior during
824 paleointensity experiments. J. Geophys. Res. Solid Earth 116, 1–12.
825 doi:10.1029/2011JB008369

826 Paterson, G.A., Tauxe, L., Biggin, A.J., Shaar, R., Jonestrask, L.C., 2014. On improving the
827 selection of Thellier-type paleointensity data. Geochemistry, Geophys. Geosystems 15,
828 1180–1192. doi:10.1002/2013GC005135

829 Pavon-Carrasco, F.J., Osete, M.L., Torta, J.M., De Santis, A., 2014. A geomagnetic field
830 model for the Holocene based on archaeomagnetic and lava flow data. Earth Planet.
831 Sci. Lett. 388, 98–109. doi:10.1016/j.epsl.2013.11.046

832 Poletti, W., Biggin, A.J., Trindade, R.I.F., Hartmann, G.A., Terra-Nova, F., 2018. Continuous
833 millennial decrease of the Earth's magnetic axial dipole. Phys. Earth Planet. Inter. 274,
834 72–86. doi:10.1016/J.PEPI.2017.11.005

835 Riisager, P., Riisager, J., 2001. Detecting multidomain magnetic grains in Thellier
836 palaeointensity experiments. Phys. Earth Planet. Inter. 125, 111–117.

837 Roberts, A.P., Pike, C.R., Verosub, K.L., 2000. First-order reversal curve diagrams: A new
838 tool for characterizing the magnetic properties of natural samples. J. Geophys. Res.
839 105, 461–475. doi:10.1029/2000JB900326

840 Roberts, A.P., Tauxe, L., Heslop, D., Zhao, X., Jiang, Z., 2018. A Critical Appraisal of the
841 "Day" Diagram. J. Geophys. Res. Solid Earth 123, 2618–2644.
842 doi:10.1002/2017JB015247

843 Rogers, J., Fox, J.M.W., Aitken, M.J., 1979. Magnetic anisotropy in ancient pottery. Nature
844 277, 644–646.

845 Selkin, P.A., Tauxe, L., 2000. Long-term variations in palaeointensity. Philos. Trans. R. Soc.
846 A Math. Phys. Eng. Sci. 358, 1065–1088. doi:10.1098/rsta.2000.0574

847 Shaar, R., Ben-Yosef, E., Ron, H., Tauxe, L., Agnon, A., Kessel, R., 2011. Geomagnetic field
848 intensity: How high can it get? How fast can it change? Constraints from Iron Age
849 copper slag. Earth Planet. Sci. Lett. 301, 297–306. doi:10.1016/j.epsl.2010.11.013

850 Shaar, R., Ron, H., Tauxe, L., Kessel, R., Agnon, A., Ben-Yosef, E., Feinberg, J.M., 2010.
851 Testing the accuracy of absolute intensity estimates of the ancient geomagnetic field
852 using copper slag material. Earth Planet. Sci. Lett. 290, 201–213.
853 doi:10.1016/j.epsl.2009.12.022

854 Shaar, R., Tauxe, L., Ben-Yosef, E., Kassianidou, V., Lorentzen, B., Feinberg, J.M., Levy,
855 T.E., 2015. Decadal-scale variations in geomagnetic field intensity from ancient Cypriot
856 slag mounds. Geochemistry, Geophys. Geosystems 16, 195–214.
857 doi:10.1002/2014GC005455

858 Shaar, R., Tauxe, L., Goguitchaichvili, A., Devidze, M., Licheli, V., 2017. Further evidence of
859 the Levantine Iron Age geomagnetic anomaly from Georgian pottery. Geophys. Res.
860 Lett. 44, 2229–2236. doi:10.1002/2016GL071494

861 Shaar, R., Tauxe, L., Ron, H., Ebert, Y., Zuckerman, S., Finkelstein, I., Agnon, A., 2016.
862 Large geomagnetic field anomalies revealed in Bronze to Iron Age archeomagnetic data
863 from Tel Megiddo and Tel Hazor, Israel. Earth Planet. Sci. Lett. 442, 173–185.
864 doi:10.1016/j.epsl.2016.02.038

865 Stillinger, M.D., Feinberg, J.M., Frahm, E., 2015. Refining the archaeomagnetic dating curve
866 for the Near East: New intensity data from Bronze Age ceramics at Tell Mozan, Syria. J.
867 Archaeol. Sci. 53, 345–355. doi:10.1016/j.jas.2014.10.025

868 Tauxe, L., 2010. Essentials of Paleomagnetism. Univ. of California Press, Berkeley.

869 Tauxe, L., Staudigel, H., 2004. Strength of the geomagnetic field in the cretaceous normal
870 superchron: New data from submarine basaltic glass of the Troodos Ophiolite.
871 Geochemistry, Geophys. Geosystems 5. doi:10.1029/2003GC000635

872 Tema, E., Hedley, I., Fasnacht, W., Peege, C., 2018. Insights on the geomagnetic secular
873 variation in the Eastern Mediterranean: First directional data from Cyprus. Phys. Earth
874 Planet. Inter. 285, 1–11. doi:10.1016/J.PEPI.2018.10.001

875 Tema, E., Kondopoulou, D., 2011. Secular variation of the Earth's magnetic field in the
876 Balkan region during the last eight millennia based on archaeomagnetic data. Geophys.
877 J. Int. 186, 603–614. doi:10.1111/j.1365-246X.2011.05088.x

878 Thellier, E., Thellier, O., 1959. Sur l'intensité du champ magnétique terrestre dans le passé
879 historique et geologique. Ann. Geophys. 15, 285–378.

880 Yang, S., Shaw, J., Rolph, T., 1993. Archaeointensity Studies of Peruvian Pottery-from 1200
881 B.C. to 1800 A.D. J. Geomagn. Geoelectr. 45, 1193–1207.

882 Yu, Y., 2011. Importance of cooling rate dependence of thermoremanence in paleointensity
883 determination. J. Geophys. Res. Solid Earth 116. doi:10.1029/2011JB008388

884 Yu, Y., Dunlop, D.J., 2003. On partial thermoremanent magnetization tail checks in Thellier
885 paleointensity determination. J. Geophys. Res. 108. doi:10.1029/2003JB002420

886 Yu, Y., Tauxe, L., Genevey, A., 2004. Toward an optimal geomagnetic field intensity
887 determination technique. Geochemistry, Geophys. Geosystems 5.
888 doi:10.1029/2003GC000630

889 Yutsis-Akimova, S., Gallet, Y., Amirov, S., 2018a. Rapid geomagnetic field intensity
890 variations in the Near East during the 6th millennium BC: New archeointensity data from
891 Halafian site Yarim Tepe II (Northern Iraq). Earth Planet. Sci. Lett. 482, 201–212.
892 doi:10.1016/J.EPSL.2017.11.013

893 Yutsis-Akimova, S., Gallet, Y., Petrova, N., Nowak, S., Le Goff, M., 2018b. Geomagnetic field
894 in the Near East at the beginning of the 6th millennium BC: Evidence for alternating
895 weak and strong intensity variations. Phys. Earth Planet. Inter. 282, 49–59.
896 doi:10.1016/J.PEPI.2018.07.002

897

***Highlights (for review)**

- Large swing to shallow inclinations in Turkey (~1900 BC) is corroborated
- Longest sequence of intensity records from Tell Acthana potsherds (2100-1350 BC)
- Intensity high over the Levant (LIAA) is confirmed with 2 new datasets from Turkey

Extreme geomagnetic field variability indicated by Eastern Mediterranean full-vector archaeomagnetic records

P. Ertepinar[1], M. L. Hammond[2], M. J. Hill[3], A. J. Biggin[3], C. G. Langereis[1], A. I. R. Herries[4], K. A. Yener[5], M. Akar[6], , M.–H. Gates[7], T. Harrison[8], A. M. Greaves[9], D. Frankel[4], J. M. Webb[4], İ. Özgen[7], G. B. Yazicioglu[10]

1. Paleomagnetic Laboratory Fort Hoofddijk, Department of Earth Sciences, University of Utrecht, Budapestlaan 17, 3584 CD Utrecht, the Netherlands
P.Ertepinar@uu.nl
2. Sustrans Scotland, Rosebery House, 9 Haymarket Terrace, Edinburgh EH12 5EZ, UK
3. Geomagnetism Laboratory, Department of Earth, Ocean and Ecological Sciences, University of Liverpool, Liverpool L69 7ZE, UK.
4. The Australian Archaeomagnetism Laboratory, Department of Archaeology and History, La Trobe University, Melbourne Campus, Bundoora, 3086. VIC, Australia
5. Institute for the Study of the Ancient World, New York University, 15 East 84th St. New York, NY 10028, USA
6. Department of Archaeology, Faculty of Arts and Sciences, Mustafa Kemal University, 31060 Antakya, Hatay, Turkey
7. Department of Archaeology, Faculty of Humanities and Letters, Bilkent University, 06800 Bilkent, Ankara, Turkey
8. Department of Near and Middle Eastern Civilizations, University of Toronto, Toronto, Canada
9. Department of Archaeology, Classics and Egyptology, University of Liverpool, Liverpool L69 7WZ, UK.
10. Division of the Humanities, Near Eastern Languages and Civilizations, The University of Chicago, Chicago, Illinois 60637, USA

Abstract

The magnetic field of the Earth can exhibit considerable variations at short time scales, even as short as decades. The archaeomagnetic studies of Middle Eastern artefacts (mainly from Israel and Jordan) show evidence for an exceptionally high intensity period from 1050-700 BC which displays two distinct spikes over the Levant, the Levantine Iron Age Anomaly (LIAA). Its exact duration and geographical extent are still poorly known. Despite the wealth of ancient settlements, the extensive cultural heritage and a long history of trade and immigration, the archaeomagnetism of Turkey and Cyprus remains largely unexplored. This study presents a large data set of ancient directions and intensities from seven archaeological sites in the Eastern Mediterranean covering a time span of ~2000 years. The recorded directions from thirteen sets of samples are coherent with our earlier findings, yet

show significantly larger swings than existing field models. In particular, we confirm the very large swing in inclination we found earlier, from 1910-1850 BC, that is also captured by the Greek PSV curve, and shallower by more than 10° than predicted by existing field models. Consequently, these models require substantial revision in this region. We were able to determine the archaeointensity from five sets of mud-bricks, from the thirteen attempted, allowing us to provide the full field vector. Furthermore, we present thirty-one new archaeointensity results from potsherds and mud-bricks that considerably enhance existing data, especially when a set of strict selection criteria is applied. Fourteen sets of potsherds from a single site (Tell Atchana) provide the longest sequence recorded so far in Turkey, from 2100 to 1350 BC. We find exceptionally high intensities of 145 and 175 ZAm^2 around 700 BC, in well-dated mud-bricks and potsherds from two different locations (Tell Tayinat and Kilise Tepe), supporting extreme geomagnetic field variability in the region. Moreover, these two high intensities confirm the younger spike of the LIAA in Turkey.

Keywords: Archaeomagnetism, archaeointensity, Turkey, Cyprus, geomagnetic spike, Levantine Iron Age Anomaly

1. Introduction

Archaeomagnetism studies burnt or fired archaeological artefacts to help understand short term variations of the Earth's magnetic field (palaeosecular variation; PSV) over the last 8,000 years or so, PSV studies are important for understanding the geodynamo that maintains the Earth's magnetic field while good PSV curves for a region can help to date certain archaeological artefacts. Archaeological features that are commonly studied include *in-situ* features such as kilns, ovens and hearths, which can provide geomagnetic field directions and palaeointensity, and *ex-situ* artefacts like tiles, bricks and ceramics that can only be used for palaeointensity studies (Thellier and Thellier, 1959).

The importance of archaeomagnetism in revealing short term changes in the strength of the geomagnetic field, such as the Levantine High, has been highlighted in recent years by studies from Syria and Iran (Gallet et al., 2015, 2014, 2008, 2006; Gallet and Butterlin, 2015; Genevey et al., 2003; Stillinger et al., 2015), Jordan, Israel and Georgia (Ben-Yosef et al., 2017, 2009, 2008a, 2008b; Shaar et al., 2017, 2016, 2015, 2011), Turkey (Ertepinar et al., 2016, 2012), and Iraq and Cyprus (Shaar et al., 2015; Tema et al., 2018; Yutsis-Akimova et al., 2018a, 2018b). The focus of recent research has been on the Middle East between ~3000-0 BC partly because Gallet et al. (2006) suggested that PSV may have played a role in controlling climate, related to what they called four 'archaeomagnetic jerks' recorded in French and Middle Eastern data. An archaeomagnetic jerk was defined as a period of high field intensity coinciding with a sharp cusp in geomagnetic field direction (Gallet et al., 2003); it is also referred to as a 'geomagnetic spike' when the high field intensity periods occur in relatively short episodes (Ben-Yosef et al., 2009). The three oldest intensity highs are proposed to have occurred based on data from Syria and Iran (Gallet et al., 2006). The fourth and youngest interval at 1050-750 BC shows a significantly higher magnitude than the three older events and is now well-known as the 'Levantine Iron Age Anomaly (LIAA)' (Shaar et al., 2016). The LIAA was first discovered in the Southern Levant (Ben-Yosef et al., 2008a), and subsequently in Turkey (Ertepinar et al., 2012) and Georgia (Shaar et al., 2017). The LIAA is

seen as a short period of exceptionally high field intensities producing VADM (virtual axial dipole moment) values in excess of 200 ZAm^2, and appears to show two distinct spikes at ~980 BC and ~740 BC (Shaar et al., 2016). However, the spatial extent of the high intensity spike is still not well constrained. Currently available data do not yet allow determination of whether the LIAA is a rapid regional perturbation or is a global scale phenomenon, and whether it is represented by single or multiple high field episodes.

A better knowledge of the evolution of the geomagnetic field in space and time would allow a better understanding of geodynamo processes as well as enabling the construction of better field models and constraining regional PSV curves to establish the nature of such high field episodes. In order to acquire this knowledge, full vector field information is required from as many different locations and times as possible. There is still a lack of published work in this area centered in Turkey and Cyprus, despite their extensive cultural heritage and a long history of trade and immigration. Abundant Cypriot slag deposits have recently been exploited as a reliable recorder of the geomagnetic field and have the potential to provide a very high resolution time series (Ben-Yosef et al., 2008a; Shaar et al., 2010), However, the data from this region are still scarce. Spatially, Turkey and Cyprus (including the Mediterranean Sea) cover a very large area that is almost the same size as one third of Europe. Considering the scarcity of the data from the region, it is inevitable that geomagnetic field models are relatively unconstrained by local data and rely heavily on data published for Bulgaria (Kovacheva et al., 2014), Greece (De Marco et al., 2014; Tema and Kondopoulou, 2011) and the Middle East. This study presents a new and large dataset of palaeodirections and palaeointensities from archaeological sites in Turkey and Cyprus, spanning the time interval from 2700 to 750 BC, the period suggested to include at least four high intensity episodes. The results help to better constrain the LIAA (1050-700 BC) at ~750 BC, to narrow the data gap over Turkey and Cyprus, and to increase the accuracy of global field models.

2. Archaeological Context and Sampling

We have sampled seven archaeological sites, two in Cyprus and five in Turkey (Fig. 1). The Cypriot sample sets consist solely of potsherds while the sample sets from Turkey consist of both potsherds and oriented samples. All potsherd sets were selected from previously excavated collections. Dependent on the availability of material, we selected sets of potsherd samples containing 6-15 samples (but occasionally only 1 or 2) per archaeological context/level (Table 1a). For oriented samples, a water-cooled drill was used to take cylindrical cores of 2.5 cm diameter and a magnetic compass was used to orient the cores *in situ*. Cores were drilled at different orientations in order to detect any anisotropy effect if present. If core length permitted, more than 1 specimen was cut from the core. Oriented sample sets contain 7-36 samples and 7-46 individual specimens per age/level (Table 1b). The majority (fifteen) of the oriented sets are sampled from surfaces that were exposed to fire, such as destruction levels or fire places. The remaining five sets are from a stratigraphic sequence of palace pavements and made from manufactured mud-bricks. These palace pavement mud-bricks did not experience any subsequent fire event and would only have been baked (or sun-dried) during manufacture. They are sampled for palaeointensity measurements and inclination-only analysis (explained in detail in the following sections).

The age of the archaeological sites, contexts or level mostly rely on the ^{14}C dates, pottery typology and relative chronology. Below we briefly describe the sampling sites; detailed information and references are given in the Supplementary Material.

Bellapais Vounous (Cyprus). Six Red Polished Ware sherds (BV-P) have been studied here (Fig. S1); all date from the Early Cypriot I-II period (2250-2100 BC).

Marki Alonia (Cyprus). We studied twenty-eight pottery sherds with various typologies (MA-P) which have been taken from contexts dated between 2400-1900 BC (Fig. S1, Table S1).

Hacımusalar Höyük (Turkey). We sampled three different levels from ~3 m high North-South trending trench where HM1 (fallen mud-bricks) and HM2 (a clay pit) are the uppermost and lowermost destruction levels dating back to Early Iron (1200-1000 BC) and Early Bronze Ages (3300-2100 BC), respectively. The third level HM3 (mud-bricks) is stratigraphically between the two levels, closer to HM2 (Fig. S2).

Kilise Tepe (Turkey). We studied eight potsherds (KIT-P) from five different occupation levels over an age interval of 1350-30 BC (Fig. S3).

Kinet Höyük (Turkey). We collected two sets of mostly mud-brick (and some serpentinite) samples from the eastern terrace of the mound (KN1 and KN2) which date back to 2000-1750 BC and 1750-1550 BC (Fig. S4).

Tell Atchana (Turkey). The stratigraphy of Tell Atchana has been subdivided into a sequence of eighteen occupation levels (Level 0 to Level XVII/XVIII, 2200-1305 BC). We have chosen 128 potsherds (TA-P), from fourteen levels as being representative of the variety in pottery typology found on the site (Fig. S5a). We additionally sampled fourteen sets (mud-bricks, basalts and an ash layer) for the full vector analyses (Fig. S5b). Five of these sets belong to a stratigraphic sequence of levels of palace pavements that were analysed for both archaeointensity and inclination only, assuming that the bricks were horizontally fired during manufacture, instead of sun-dried. This assumption is tested in the following sections.

Tell Tayinat (Turkey). We collected one mud-brick set (TT1) from the burnt Iron Age II temple that was destroyed by an intense fire at ~672 BC (Fig. S6).

3. Rock Magnetic Experiments and Results

Rock magnetic properties such as the room temperature bulk susceptibility, Isothermal Remanent Magnetisation (IRM) acquisition, hysteresis loops, first order reversal curve (FORC) diagrams and Curie curves are measured using a Kappabridge KLY-2, an

alternating gradient force magnetometer, and a modified horizontal translation type Curie balance (Mullender et al., 1993).

The IRM experiment results on potsherds (Fig. 2a) indicate that all samples contain a low coercivity phase and are saturated in fields well below 300 mT. All curves except for one (BV-P) showed almost fully reversible heating curves if heated up to ~600°C; occasionally, some alteration (oxidation) occurred if heated to 700°C, producing a slightly lower intensity in the final cooling curve. All curves from BV-P, MA-P and TA-P have a change in slope at or close to 580°C, and hence the inferred dominant magnetic carrier is magnetite. Four of the eight KIT-P samples show two Curie temperatures (T_c), the first at ~300°C, the second at ~580°C implying the presence of both Ti-rich titanomagnetite and magnetite. Three of the other samples have curved thermomagnetic curves where it is impossible to isolate a T_c. The remaining one sample has a T_c of ~550°C due to the presence of Ti-poor titanomagnetite. These interpretations are supported by the low coercivities (B_c=6-14 mT) observed in the samples (Fig. 2a).

The IRM acquisition and hysteresis loop experiments on oriented cores showed that all samples saturate and the loops close at fields generally well below 200 mT, while generally low coercivities (B_c=4-24 mT) are observed in the samples, supporting magnetite as carrier (Fig. 2a). The thermomagnetic curves are measured in air up to 700°C that include heating and cooling cycles to check the occurrence of chemical alteration. The applied field varied from 100/180-300 mT. All sets display similar and fully reversible heating/cooling curves up to 600°C indicating that the magnetic minerals are chemically stable up to the Curie temperature of magnetite. Only upon heating to 700°C some oxidation occurs resulting in a slightly lower final cooling curve. For all basalts (TA) and mud-bricks (HM, KN, TT and the majority of TA), the highest T_c is at ~580°C pointing to magnetite as the main magnetic carrier. A small number of mud-bricks from the palace pavements (TA14-TA18) on the other hand, have a Curie temperature varying from ~500 to 580°C which indicates the presence of some low-Ti titanomagnetite. The samples from the ash layer (TA3) have a slightly higher T_c

of ~600°C which points to some cation deficient magnetite. In some of the curves from the mud-bricks and the ash layer, the heating curves display a second inflexion in the range 350-420°C, which can be interpreted as Ti-rich titanomagnetite as a second carrier. The clay furnace from Hacımusalar (HM2) and the clay pot from Tell Atchana (TA5) showed rock magnetic properties identical to the mud-bricks from the sites. Therefore, they are not displayed in figure 2a; instead they are grouped with the other mud-bricks hereafter.

For all samples, after removal of the paramagnetic contribution, we determined the ratios of remanent saturation magnetisation to saturation magnetisation M_{rs}/M_s, and the remanent coercive force to coercive force H_{cr}/H_c and plotted them in a Day plot (Day et al., 1977) as modified by Dunlop (2002) (Fig. 2b, Table S2) even though such a diagram may not sufficiently resolve the domain state of the magnetic particles (Roberts et al., 2018). The majority of the potsherds and mud-bricks are in the PSD part of the Day plot but above the SD-MD mixing lines with the exception of seven TA-P and one KIT-P potsherd that plot outside the PSD (and MD) field. The hysteresis ratios from MA-P and KIT-P potsherds plot within the distribution of the TA-P samples but their distribution is slightly more to the right (higher H_{cr}/H_c ratios) implying that these sherds are very similar to the somewhat coarser magnetic minerals of the TA-P distribution. Mud-bricks from KN and TT and the basalt samples from TA produced similar hysteresis ratios plotting in the PSD area but towards the SD field of the plot, implying generally finer-grained magnetic materials. For further (palaeointensity) analyses we discarded eight potsherds with non PSD/SD assemblage and one potsherd with an irreversible Curie curve (almost zero intensity final cooling curve due to inversion of maghemite to hematite at ~350°C).

A FORC diagram is also useful to assess the domain state of magnetic minerals and the local interaction fields for an assemblage of magnetic particles. It provides an additional check on the reliability of the hysteresis parameters such as the M_{rs}/M_s ratio which can be altered by a mixture of domain assemblages (Roberts et al., 2000). Out of 35 measurements, one representative sample from each set is shown in figure 2a. All B_c results are in

agreement with what is derived from the hysteresis experiments. The mud-brick sets KN, TA and TT have two closed inner contours with peaks at ~10 mT with narrow vertical spreading of the contours indicating that the assemblages are dominated by non-interacting PSD grains. The basalt samples have a peak at B_c=25 mT with four closed inner contours where, except for the outermost contour, all the inner contours have narrow spreading along the B_u axis which is typical for PSD grains. The ash layer from TA exhibits a distribution with a peak centered about the origin.

The low field bulk magnetic susceptibility values range between 1.55×10^{-5} to 4.02×10^{-2} SI, the majority (96%) being higher than 1.00×10^{-3} SI. The results are used to calculate the Koenigsberger ratio, Q_n, which is defined as the ratio of remanent to induced magnetisation that indicates a rocks capability to carry a stable remanence, in this case the TRM. All types of materials including the minor amount of low susceptibility samples have Q_n>1, indicating that the samples have a stable TRM (Fig. S8).

4. Archaeomagnetic Direction Determination

4.1. Demagnetisation

The analysis of the Natural Remanent Magnetisation (NRM) directions, all statistics and field tests were done through the on-line portal Paleomagnetism.org (Koymans et al., 2016). The portal uses orthogonal projection diagrams, eigenvector analysis and Fisher (1953) means. The acceptance limit of maximum angular deviation (MAD) of individual directions is taken as 10° although was typically MAD<2°, while only means with k>50 are accepted (Table 2a, Figs. 3a and 4). We regard the results as a characteristic remanent magnetisation (ChRM). We also use a test for a common true mean direction based on the coordinate bootstrap test of Tauxe (2010) which randomly samples two distributions of directions and converts those to Cartesian coordinate (x, y, z) distributions. The test is positive if all three Cartesian distributions overlap at the 95% level.

For the directional analysis, sets of 7 to 20 samples from each site are demagnetised by both thermal (2G Enterprises DC-SQUID cryogenic magnetometer) and alternating field (high precision robotized DC-SQUID magnetometer) techniques with incremental steps of 50°C up to 580-600°C or 2-5 mT up to 100 mT.

One representative demagnetisation diagram from each type of building material along with the decay curves are plotted in Figure 3a. For all sets, the viscous component is removed at low temperatures (~180-210°C) or coercivities (~10 mT). The remanence is nearly completely removed at ~580°C or 100 mT and usually decays straight to the origin. These findings from the demagnetisation diagrams and intensity decay curves are coherent with the general findings from the rock magnetic experiments, although the inflexion observed in the Curie curves from the ash layer (TA3) is not seen in the demagnetisation decay curves. Occasionally, for some sister specimens from the bottom part of the oriented core, we took the component that was heated to a sufficiently high temperature. For example, TA2.13B was clearly only heated up to 500-525°C by the destruction fire, but up to that temperature giving a component that was identical to the highest temperature component of other samples from the same site (Fig. 3a). Thermal and AF demagnetisations produced identical directions as shown by the positive coordinate bootstrap test of Tauxe (2010) (Fig. 3b) . All ChRM results per site are corrected for the International Geomagnetic Reference Field (IGRF) declination at the position and time of sampling and are shown in Figure 4.

4.2. Directional Results

Hacımusalar Höyük. The demagnetisation diagrams of all sets display a stable NRM decaying to the origin. Two out of three sets (HM2 and HM3) produced acceptable results with k=104 and k=65, respectively. The relatively low k value of HM3 could be related to slight displacement of the bricks due to the thick earth cover on the top (as seen in figure S2). The demagnetisation diagrams of the third set (HM1) are also single component but

have completely random directions; hence, the collapse must have taken place after the fire event. HM1 is thus excluded from further directional analysis.

Kinet Höyük. The samples from KN1 that is composed of mud-bricks (the wall) and serpentinites (the foundation part) produced well clustered single component demagnetisation diagrams with uniform decay curves from its mud-bricks and random directions from the serpentinites. As was observed earlier by Ertepinar et al. (2016), the foundation part of the structure generally does not burn to a sufficiently high temperature to record the field. Therefore, the seven serpentinite samples are discarded, making the set of nine mud-bricks very well clustered with k=862. The samples from KN2 that is composed solely of mud-bricks also have single component demagnetisation diagrams decaying to the origin, supporting the general findings from the Curie curves. The set has a well-defined ChRM (k=366).

Tell Atchana. The sets from the site form the bulk of the directional results. Nine sets were measured for both declination and inclination and an additional five sets (repairment levels of palace pavements) were analysed for inclination only.

All mud-brick samples display an ideal magnetite magnetisation decaying straight to the origin with uniform decay curves as was also deduced from the Curie experiments (Fig. 2a). Out of five sets that are composed solely of mud-bricks, four sets (TA1, TA5, TA8, and TA9) have a well-defined ChRM direction with high k values. One mud-brick set (TA10) turned out to be not sufficiently burnt and shows random directions and is therefore excluded from further directional analysis.

The samples from the ash layer (TA3) were extremely fragile and were demagnetised only using the AF method. The NRM of the samples decay uniformly, however the remanence is not fully removed at 100 mT pointing to the presence of maghemite, which is coherent with the Curie measurements. The set has a lower k value (k=55) compared to the other sets.

This higher scatter is likely related to the fragile nature of the furnace material that makes it difficult to orient the sample.

The basalt sets (TA4 and TA19) also have single component demagnetisation diagrams where the viscous component is removed at slightly higher temperatures (~250°C). The remanence is nearly completely removed at 580°C but not yet at 100 mT, which could indicate the presence of a stable single-domain (SD) magnetite or a minor amount of maghemite (which was not observed in the Curie curves). The sets produced a well-defined ChRM with *k* values of 294 and 223, respectively.

One set that is composed of both mud-bricks and basalts (TA2) also show an extremely good cluster (*k*=979) where the directions of basalts and mud-bricks are in excellent agreement. This provides additional evidence that these mud-bricks are not strongly anisotropic.

The results of the 5 palace pavement mud-brick sets (TA14-18) are inconclusive. The high temperature/coercivity components produced 'shotgun pattern' distributions (Fig. 4). When the sets are analysed for the low temperature/coercivity component (20-150°C or 0-10 mT), there appears to be a poorly constrained cluster. When only the thermal demagnetisation results are used, there is a better cluster (with a steep inclination of 73°) but still not good enough (k=21) to give a reliable result, even though we used the 45° cut-off in Paleomagnetism.org (Fig. 4). It is likely that the palace pavement mud-bricks were baked during manufacture and as this is likely to be at a lower temperature than the destruction fires, this could result in the NRM being less stable and more prone to acquiring an overprint. Alternatively the bricks might have been randomly oriented during manufacture. Finally it is possible that the samples were not baked and instead retain a sun-dried NRM (Games, 1977). These sets are discarded from further directional analyses.

Tell Tayinat. The mud-brick samples from the single set (TT1) from the site display single component magnetite demagnetisation diagrams with a minor overprint that is removed at

210°C. The uniform decay curves and the removal of magnetisation at ~580°C are coherent with what is observed in the Curie curves. The set has a well clustered distribution (k=570).

In summary, out of 21 sets of samples collected from four different archaeological sites with a wide age interval of ~2000 years, 13 sets (at least one set from each site) were considered to be of sufficient good quality. Declinations range between 344.9° and 10.2° and inclinations between 36.0° and 62.9°.

5. Archaeointensity Determination

5.1. Archaeointensity Methods

Microwave experiments on potsherds. The 14GHz Tristan microwave system was used to conduct intensity experiments on all potsherd samples. The microwave frequency was individually tuned to optimise the absorption of each sample. Demagnetisation experiments were first conducted on each sherd prior to the intensity measurements to further determine the suitability of the sherd for intensity experiments (Fig. 3a). In total, 161 samples exhibited a single component decaying to the origin and were deemed suitable for archaeointensity experiments and 23 samples deemed unsuitable following the microwave demagnetisation and rock magnetic experiments. The majority of the unsuitable samples were rejected because they did not show a stable component of remanence decaying towards the origin. This is likely to have been caused by insufficient heating or by pot movement during firing.

For each selected potsherd, a subsample was subjected to a full microwave demagnetisation/remagnetisation experiment with a field applied parallel to the NRM. We followed either the Coe protocol (1967) or an IZZI protocol (Tauxe and Staudigel, 2004; Yu et al., 2004) (Fig. 5) with applied laboratory fields between 53 and 90 μT. As the KIT-P set was so small, all six samples were subject to both methods. Repeat partial microwave induced Thermoremanent Magnetisation (pT_MRM) checks were carried out to monitor possible alteration and repeat zero field checks were made as an additional alteration check and also

to detect Multi-Domain (MD) sensitivity when following the Coe protocol (Riisager and Riisager, 2001). It is recognised that applying the field parallel to the NRM direction will mask MD behaviour (Yu and Dunlop, 2003). The applied cooling rate (CR) correction protocol on potsherds is described in the Supplementary Material.

Thermal experiments on palace pavement mud-bricks. The samples from the mud-brick palace pavements of Tell Atchana (TA14-TA18) were grouped into two as University of Liverpool and Utrecht University sets.

The Liverpool experiments followed the IZZI protocol with an applied laboratory field of 53 μT, either sub-parallel or anti-parallel with additional alteration checks. Up to fourteen double heating steps were applied between 100°C and 525°C with pTRM checks after every second step.

The Utrecht set is measured with an applied laboratory field of 50 μT in a temperature range of 20-420°C. The experiments involved seven double heating steps and were performed using the IZZI protocol with the applied field randomly oriented with respect to the NRM of the sample. The measurements were carried out with one pTRM check, enabled after the final double heating step of the experiment (Fig. 5). The CR corrections on pavement bricks are described in the Supplementary Material and show that CR effects are minimal.

Combined microwave and thermal experiments on oriented mud-bricks. Mainly thermal (Utrecht) and a minor amount of microwave (Liverpool) experiments were run on six sets of mud-brick samples either following IZZI or Coe protocol with applied fields between 40 and 100 μT. Microwave experiments were carried out with the applied field parallel or anti-parallel to the NRM of the samples, whereas thermal experiments were performed using a custom built orientation tray that enables aligning samples individually to desired angles, in this case parallel to the NRM. In the microwave experiments, pTRM checks were performed after every double treatment to monitor the possible influence of alteration. Thermal experiments

were carried out with pTRM checks either fully enabled in every two double heating steps or one successful check at the end of the experiment (Fig. 5).

Due to the lengthy nature of CR experiments we did not investigate the effect of cooling on these data sets, however, based on earlier results (Biggin et al., 2013; Yu, 2011), our previous experiments on the PSD mud-bricks (Ertepinar et al., 2012), our results on the Tell Atchana pavement mud-bricks from this study and the consistency between microwave and thermal experiments which have very different cooling times suggest the CR effects are minimal and hence can be neglected.

5.2. Anisotropy Determination

Pottery has been shown to be strongly anisotropic (Chauvin et al., 2000) due to the preferential alignment of magnetic grains presumed to be induced during the creation of the ceramic artefact. For both wheel and hand-made pottery, if the clay is worked into a particular orientation it is probable that the plate-like clay particles become aligned during fabrication and cause a similar alignment of the magnetic minerals (Yang et al., 1993) that can lead to an error in the intensity estimation of up to 50% (Gómez-Paccard et al., 2019). In order to mitigate the effects of anisotropy, the field was applied parallel to the NRM direction (Rogers et al., 1979). The effectiveness of this method is further confirmed by Odah et al. (2001) who determined accurate palaeointensities from experimentally manufactured ceramics. As an additional check, the angle γ between the pTRM acquired at the last step used for the best-fit segment and the applied field direction (Biggin and Paterson, 2014) was checked for all potsherds and also the mud-bricks.5.3. Selection criteria

For both microwave and thermal experiments, following criteria are followed:

1. The number of points (N) defining the slope: $N \geq 5$
2. The ratio of standard error of the slope to absolute value of the slope $\beta < 0.1$ (Selkin and Tauxe, 2000)

3. The lower acceptance limit for the NRM fraction: f≥0.35 (Coe et al., 1978). However, except for two measurements, f values are much higher
4. The acceptance criterion of quality factor (q) is 3
5. The upper acceptance limits for the angle between anchored and non-anchored best-fit vector (α) (Selkin and Tauxe, 2000) is taken as 10°
6. MD behaviour of the interpreted segment of the NRM-TRM plot is assessed by the curvature statistics, $|k'|$, and the acceptance limit is taken as 0.164 as suggested by Paterson (2011), but we accepted two sherds with $|k'|$=0.169
7. pTRM checks (where applicable) were deemed to have been successful if the ratio of the difference between the check and the relevant TRM value to the length of the selected NRM-TRM segment (DRAT) was smaller than 10% (Selkin and Tauxe, 2000) and the cumulative DRAT (CDRAT), defined as the sum of all the DRATs, should be less than 11% (Paterson et al., 2014)

5.4 Archaeointensity Results

Potsherds. Archaeointensity experiments on potsherds were carried out on 114 individual sherds from Tell Atchana (TA-P), 6 from Kilise Tepe (KT-P), 5 from Bellapais Vounous (BV-P) and 22 from Marki Alonia (MA-P). We did experiments on an additional 14 sister samples (Table S3a).

From TA-P, 56 out of 114 individual potsherds (57 measurements) passed all the criteria yielding a success rate of 49%. The values for the angle γ is found to be <5° for the majority (forty-five) of the potsherds, eight have 5°<γ<10° and the remaining four have γ>10°. On average, the CR correction factor was 0.85 with the largest correction factor being 0.73 for Level IV. An unusual positive correction factor of 1.08 was recorded for Level XVII/XVIII. For the majority of levels it was only possible to carry out one CR correction experiment. The site mean (CR corrected) intensity values from the potsherds of TA-P range from 39.8 to 55.1 μT. Over the duration of the occupation of the site (2200-1300 BC) the field fluctuated between

409 this maximum and minimum. The highest field value of 55.1 μT was recorded for the
410 lowermost level (Level XVII/XVIII) which represents the earliest occupation level of the site,
411 ~2200-2000 BC, whereas the lowest value was from Level IX (1675-1575 BC) (Table 2b).

412 The results from KIT-P have a much lower success rate (38%) on specimen basis, where
413 one to two sister specimens from each sherd failed to meet the acceptance criteria. The set
414 with the largest age interval (level I/II) did not provide any successful result from two
415 measurements on the single sherd from the level. Two sets, levels IIa and IId, produced one
416 successful result each, where both measurements are of good quality with similar (and high)
417 intensity values of 83.2 and 84.1 μT, respectively. Unfortunately, no samples from these sets
418 survived for the CR experiments. The fourth set (level IIe) again did not provide any result
419 from the single sherd. The final set, level IIf (800-650 BC), produced a CR corrected mean
420 intensity value of 81.9 μT from three successful measurements performed on two sherds.
421 Individual CR measurements on these sherds are found to be 0.84 and 0.82. The angle γ for
422 the successful measurements is found to be 3.4° on average (highest being 6.3°).

423 Out of a sample set of 27 Cypriot sherds, 14 gave acceptable results, (success rate of 52%).
424 The site MA-P had the largest variety of pottery typology among all sites. It is noted that
425 there is no apparent pattern in the samples that were unsuccessful/successful which could
426 be related to pottery type. The first group of samples consisting of Red Polished Ware, Red
427 Polished Coarse Ware and Drab Polished Ware produced a CR corrected archaeointensity
428 value of 38.8 μT from five potsherds out of thirteen. The second set was composed of only
429 one Red Polished Ware sherd from Early Cypriot I-II where the CR corrected intensity value
430 is 53.0 μT from a single measurement. The oldest set with Red Polished Philia Ware yielded
431 four acceptable results out of nine with a mean CR corrected intensity value of 53.8 μT. The
432 experiments run on the potsherds from BV-P produced a CR corrected mean intensity value
433 of 46.4 μT from four potsherds out of five. The correction factor of 0.83 was adapted from the
434 same pottery type of MA-P (Red Polished Ware) since all potsherds showed sign of
435 alteration (Table S3a). The angle γ is <6.6° for the accepted Cypriot potsherds (2.6° on

436 average). In all cases, the intensity determined was consistent with the other results for the
437 level (Table S3). We therefore conclude that anisotropy is not biasing our results.

438 For some potsherd levels there is a significant range in intensity values. For example, TA-P
439 Level II/III has a range of 15.7 μT, while Level XVII/XVIII has 21.5 μT and MA-P Early Cypriot
440 II/Middle Cypriot I level has 24.4 μT. Correspondingly, the standard deviations are high even
441 though in some cases one single value determines the large range. For example, if we
442 disregard the 43.2 result in the TA-P Level II/III the range becomes 3.5 μT.

443 *Mud-bricks.* Of all 66 mud-brick samples only 18 failed, implying a high success rate of 73%.
444 Of the 18 failed samples, 12 failed for a combination of criteria, but 6 failed due to the
445 curvature parameter only.

446 The mud-brick samples from the palace pavements (TA14-TA18) gave no useful directional
447 data, but gave consistent archaeointensity results with very little zigzagging in the NRM-TRM
448 plots. This suggests that the mud-bricks were manufactured in random orientations rather
449 than having an unstable NRM or being sun-dried. The sets have a very high success rate of
450 85%. For the youngest (TA14) and oldest (TA15) levels we did not perform the CR
451 experiment. However, from the three sets where we did establish a CR factor for each set,
452 the intensities were 1.3-2.4 μT lower, well within the standard deviation. Hence, CR effects
453 are minimal for this data set, in line with our earlier conclusions (Ertepinar et al., 2016). The
454 highest and lowest mean intensity recorded are 45.2 and 37.7 μT (Table 2b, Table S3b).

455 Out of six sets of mud-bricks -which all gave good directional results- five sets gave
456 acceptable archaeointensity results from at least two samples per set, only one set (TA5)
457 failed. For all the accepted results, the angle γ is found to be <5.3°, suggesting that the
458 anisotropy effects are minimal. The highest success rates of 83.3% and 67% are from TA
459 Level 4 and Level 7 Palace samples, respectively. The mean intensity values for the sets are
460 67.2 and 65.9 μT.

The single set from Tell Tayinat (TT1, ~672 BC) produced two successful thermal results (out of four) with a mean intensity value of 96.7±2.1 μT. The fifth measurement (microwave) yielded an unrealistic overshoot result (482.5 μT) which failed in the curvature parameter, |k'|.

The two remaining passed sets are from Kinet Höyük (KN1 and KN2). Samples from KN1 had an indestructible NRM and therefore the NRM fraction (f) remained much lower than the acceptance limits even when high powers were applied, that caused a melting spot indicating alteration. The success rate for the level is 25% (6 rejections out of 8). The two successful results (one TT and one MW) are in good agreement with each other with a mean intensity value of 55.2±0.9 μT. Thermal measurements on two samples from KN2 gave a mean intensity value of 64.9±1.2 μT (Table 2b).

6. Discussion

6.1 Directions

The majority of the directional data presented in this study (Figs. 6a and b) are from an age interval (mostly 1875-1465 BC) and region that is lacking data. The new results, following the IGRF correction for the declinations, are plotted against the data from Geomagia50.v3.2 (downloaded on December 2018) (Brown et al., 2015), the data from Turkey, Cyprus and Israel (Ertepinar et al., 2016, 2012; Shaar et al., 2016; Tema et al., 2018) and the global field model SHA.DIF.14k (Pavon-Carrasco et al., 2014). The data are relocated to and the models are calculated at Kayseri (38.85°N, 35.63°E), the approximate center of Turkey.

The declinations from the youngest data set TT1 is more to the west (D=350.2±4.2) compared to the predictions of the model SHA.DIF.14k, although it just overlaps within error the westward swing seen in the model, but the direction is in excellent agreement with the near contemporaneous data point (D=349.5±8.5) from (Ertepinar et al., 2012). These two data points, which are well constrained in age, confirm the existence of a westerly swing suggested to have occurred between 780-690 BC by SHA.DIF.14k. The inclination value of

the site (I=62.7±2.7) is slightly shallower than predictions of SHA.DIF.14k (~4.5°), but again in excellent agreement with the Ertepinar et al. (2012) inclination (I=61.8±5.5).

There are ten data points from 1650-1465 BC (all TA sets, KN2 and HM3) that show a trend from east (~10°) to west (~-15°), towards younger ages, with the exception of one single data point (TA5). The declination curve from SHA.DIF.14k has a very similar trend from 1800 to 1450 BC in approximately the same age interval, from ~7° east to ~5° west, and the model is coherent with the trend of our new data points. However, the westernmost and easternmost declination values of our data are exaggerated by some 5-10° compared to the model curve which is likely due to the inherent smoothing in constructing the model. The reason for the misfit declination of TA5 is likely related to our (apparently unsuccessful) attempt to restore the directions of the *ex-situ* hearth to its original position relying on the grid plans (Fig. S5b). For the age interval of our data points, SHA.DIF.14k predicts a continuous increase in the inclination where our data are in good agreement with this increasing trend. Data points TA2, TA4 and TA19 would fit better with the model when plotted on the younger end of their age uncertainty. This could be a reasonable interpretation considering all three sets are from the same heavily burnt destruction level which ended the Level VII era. The trend in inclination is in excellent agreement with a similar trend in inclination from Ertepinar et al. (2016). Also our inclinations are exaggerated, by some 10°, because of model smoothing.

The direction from KN1 plots perfectly in line with the Ertepinar et al. (2016) data, both in declination and inclination, slightly to the west of SHA.DIF.14k predictions. The inclination value of the set is 10-15° shallower than the model predictions but in good agreement with Geomagia50.v3.2 data within a few degrees.

The oldest data point HM2, displays a direction consistent with the model, but this is largely due to the large errors in declination and inclination, while the site also has an extremely large age uncertainty of ±600 years.

We then compared our new directional data to the best available PSV curves in the region, Greece (De Marco et al., 2014) and Bulgaria (Kovacheva et al., 2014), without their published error bounds for better readability (insets in Figs. 6a and b). Clearly, our youngest data (TT1) around 700 BC excellently fit the Greek curve both in declination and inclination. Between 1600 and 1300 BC there is poor to reasonable correspondence; the declination swing in our data (TA1, TA8 and TA9) is not seen in either curve, but our inclinations fit both curves reasonably well. Also our earlier swing to western declination between 2000 and 1700 BC (Ertepinar et al., 2016) is not seen in either curve, but the conspicuous swing to shallower inclinations in the Turkish data is excellently covered in the Greek curve, but not in the Bulgarian curve.

Out of the 13 sites with directional information we have the palaeointensity for 5 sites, thus providing the full field vector (Table 3).

6.2 Archaeointensities

The geomagnetic field in the Middle East over the time period from 3000-0 BC is marked by at least one period of extremely high field intensity, the LIAA (Shaar et al., 2017, 2016) dated to between 1050 and 700 BC. Shaar et al. (2017) argue that it actually consists of two spikes, with VADMs up to 180 ZAm^2, with slightly lower VADMs<140 ZAm^2 between the spikes. This high intensity was also confirmed in Turkey (Arslantepe, 176 ZAm^2, Ertepinar et al., 2012). The geographic extent of the LIAA and the exact duration of these spikes remain unclear. Recently, Shaar et al. (2016) suggested these spikes are caused by a regional anomaly which extends further to the east (Georgia, 45°E), but has a limited extension to the west, at about 30-35°E. This is mainly based on the argument of Shaar et al. (2017) that there is no evidence for the LIAA in Greece and Bulgaria. However, it is evident that there are very few data in Bulgaria in the LIAA age interval, although the slightly larger database for Greece does not show intensities >105 ZAm^2 either. The LIAA may extend further east, to Turkmenistan at 60-65°E where intensities >145 ZAm^2 are found. In their study of Holocene

lavas from the Canary Islands, de Groot et al. (2015) find high palaeointensities ~120 ZAm^2 at 826-723 BC. Recently, Béguin et al. (2019) used three marine sediment cores from the Mediterranean to better constrain the LIAA in time and space. They suggested that the LIAA moves from 40 to 55° East at 1000 BC to ~25° East at 0 CE, while decaying from ~150 to ~110 ZAm^2 in the same time span. This is partly based on the relatively low palaeointensities they find in their westernmost core in the Alboran Sea (<80 ZAm^2). However, in Portugal Nachasova and Burakov (2009) find palaeointensities higher than 140 ZAm^2 in the LIAA interval (880-730 BC) and higher than 160 ZAm^2 around 500 BC, while a recent study of Molina-Cardín et al. (2018) reports the highest intensities ever recorded in Spain, ranging 144-152 ZAm^2 around 600 BC. Earlier, Hervé et al. (2013) found high intensities for Western Europe (relocated at Paris) of more than 140 ZAm^2 around 800 BC. Interestingly, Bourne et al. (2016) find high relative palaeointensities from a cave deposit in Texas for the similar time interval (modelled at 893±135 BC). They suggest an almost four-fold increase in geomagnetic field intensity lasting several hundred years and presents evidence for the existence of an intensity high in North America that is roughly contemporaneous with the similar duration of the LIAA, although the age of the (single) spike is between the two spikes at ~980 and ~740 BC. They argue that the cave record may provide evidence for flux lobes as seen in the present-day field, and effects of the Near East lobe is mirrored by the North American lobe. Clearly, the nature of the LIAA in space and time, as a regional or global feature is still far from resolved.

This study presents thirty-one new sets of archaeointensity results, two of which are from a period of suggested high intensities. Out of thirty-one, three sets of potsherds gave only one successful result. Even though N=1 cannot by any means be considered reliable, the results from these sets are still reported (Table 2b), but displayed separately from the rest of the group (Fig. 6c). The remaining sets have successful measurements (N ranging 2 to 9). The VADM of the sets are plotted against the field model SHA.DIF.14k, the data from the Middle

East, Cyprus, Georgia, Turkey (mostly our own compilation from the respective papers) and Geomagia50.v3.2 data.

The oldest four results are from the Cypriot potsherds from an age interval of 2325-2000 BC, where BV-P produced a mean which is spot on the SHA.DIF.14k prediction; all sets, ranging 71-99 ZAm^2, are coherent with the Middle East data and within error fit the model predictions. The set with a single successful measurement (97.0 ZAm^2) is also in agreement with the Middle East data but here we have no standard deviation.

The dataset from Tell Atchana potsherds provides the first semi-continuous archaeointensity sequence from a single location in Turkey spanning the age interval 2100-1350 BC. All fourteen data points differ from SHA.DIF.14k by at most 10 ZAm^2, with the means ranging 71.9-99.4 ZAm^2. In general, the means are within error of the SHA.DIF.14k model, and nicely follow its trend for this age interval.

The five sets from Kilise Tepe gave rather disappointing results. Two sets produced no results, another two sets provided no acceptable results because of only one successful measurement. Only one set produced an acceptable result. The N=1 results from 1300 and 1150 BC (plotted dark green and transparent in Fig. 6c) are significantly higher than both models (by at least 40 ZAm^2) and much higher than the Middle East and Geomagia50.v3.2 data. The successful set consisting of three measurements has a VADM of 147±11 ZAm^2 at 725±75 BC. This result is higher than both models but in agreement with the Middle East and Georgia data and confirms the existence of the younger spike of the LIAA suggested by Shaar et al. (2017). It should be noted that even the rejected measurements from the set are consistently high, ranging 140-160 ZAm^2 (Table S3a).

Mud-brick sets from the repairment levels of palace pavements TA14-TA18 that have the highest success rate display a continuous steady decrease in the intensity from 81.6 to 68.1 ZAm^2 for the age interval between 2040 and 1675 BC, contemporaneous with the oldest ten sherd levels from Tell Atchana. There are no systematic differences observed for the

potsherds and mud-bricks results. The decrease in the intensity is extended to younger ages by some 150 years compared to SHA.DIF.14k. This trend is followed by an abrupt increase to 79.1 ZAm^2 within some 50 years. The other two mud-brick sets from TA (Levels IV and VII at 1465 and 1625 BC) are both much higher (~120 ZAm^2) than the model predictions that range 80-100 Zam^2 during this time span. Only the younger data point is consistent with some of the data from Geomagia50.v3.2.

From Kinet Höyük we have two acceptable intensity results of 98.8 ZAm^2 (KN1 at 1875 BC) and 116.1 ZAm^2 (KN2 at 1650 BC). The intensity of KN1 -although higher than SHA.DIF.14k- is in excellent agreement with the high intensities ranging 90-106 ZAm^2 found during this time by Ertepinar et al. (2016). The intensity of KN2 is similar to that of TA Level VII (118.9 Zam^2) at 1625 BC (Fig. 6c). When compared to the two potsherd results from the same age, there is a significant difference, the potsherds having lower intensities by ~45 ZAm^2, almost 40%. The cooling rate effect cannot explain this discrepancy, since the mean effect in our mud-bricks is on average 5%, in line with the majority of the estimates (mostly 4-10%) from the compilation of (Genevey et al., 2008). The older set KN1 has one microwave and one thermal measurement which are extremely consistent (Table S3b) despite the very different cooling times of a few seconds (MW) to up to an hour (TT). The VADM plot shows that the potsherd results are more consistent with Geomagia50.v3.2 data and the SHA.DIF.14k predictions. Since there is no clear preference in terms of data quality, we cannot favour any of the two results over the other two. Although very rapid changes have been shown to occur (e.g. during the LIAA), we lack sufficient data to speculate on this.

The set from Tell Tayinat (TT1) from ~672 BC has a very high intensity of 174.4 ZAm^2, and equals the highest VADMs found by Shaar et al. (2016). This confirms the LIAA younger spike to be recorded in Turkey.

Finally, we applied a number of strict criteria on Geomagia50.v3.2 data, following Poletti et al. (2018). However, we were more lenient on the age error (±250 year instead of ±100) and

615 we did not require MD monitoring. These criteria removed about 80% of the
616 Geomagia50.v3.2 data (inset in Fig. 6c). The major improvement applying the strict criteria is
617 on the age interval of 2300-1300 BC, where there is significantly less scatter. Our
618 contribution from this study doubles the available data for this time interval.

619 7. Conclusions

620 In this study, we present thirteen new directional data five of which provide the full vector of
621 the field. The recorded directions show larger swings than the models for both declination
622 and inclination, which we contribute to the inherent smoothing in the construction of the
623 models. This was also noted earlier by Ertepinar et al. (2016) who found similar larger
624 directional swings than the models. Hence, our earlier and present data contribute
625 significantly to improving the resolution of existing models, in particular for this region.

626 In addition, we provide thirty-one new archaeointensity results from both potsherds and mud-
627 bricks. The potsherds from Tell Atchana provide the longest sequence from 2100 to 1350 BC
628 recorded so far in Turkey. In general, the results agree well with existing data from the
629 Middle East, and are usually in reasonable agreement with model predictions. Applying strict
630 criteria (Poletti et al., 2018) on Geomagia50.v3.2 archaeointensity data improves the
631 resolution for the age interval of 2300-1300 BC and the data presented in this study doubles
632 the amount of high-quality data for this time interval. The conspicuous high intensity interval
633 of the LIAA is further confirmed in Turkey; in particular the younger spike of the LIAA is
634 recorded by our new data, both in well-dated mud-bricks and potsherds, from two different
635 locations (Tell Tayinat and Kilise Tepe). Earlier, we provided evidence for very high
636 intensities in the older spike of the LIAA as recorded in Arslantepe by Ertepinar et al. (2012).
637 It appears that the LIAA is a robust feature, at least in the Levant and Middle East. Its spatial
638 and temporal extents, however, require more records from geographically distinct areas.

Acknowledgements

We are grateful to Nicholas Postgate and Mara Horowitz for engaging in fruitful discussions. Nicholas Postgate is also thanked for supplying the samples from Kilise Tepe. We are grateful to Ben Claasz Coockson and people in the excavation teams who were helpful at all times. We thank Nuretdin Kaymakci -the drilling expert- who has been a great help in the field. MLH acknowledges a Natural Environment Research Council studentship held at the University of Liverpool. MJH acknowledges NERC grant NE/I013873/1. The editor and two reviewers are thanked for their thorough reviews.

Figure Captions

Figure 1. Location map of studied sites from the Mediterranean (red). Green circles are the previously published data from Anatolia and Upper Mesopotamia, Turkey. Blue circles are the data from the Middle East (see the text for references).

Figure 2. (a) Representative Curie curves, hysteresis loops (displayed after the paramagnetic correction on a mass-specific basis), IRM acquisition curves of potsherds and oriented cores from each sampling site. For all potsherds, the Curie curves are almost fully reversible, where red (blue) lines are the heating (cooling) curves, with T_c at ~580°C indicating the presence of magnetite as the main carrier. The inflexion at ~300°C in KIT-P sample points the presence of Ti-rich titanomagnetite. Samples from BV-P exhibit a paramagnetic contribution in their Curie curves and hysteresis loops. IRM acquisition curves (green lines) for all samples show saturations fields of well below 300 mT. All oriented cores display near reversible heating (red) and cooling (blue) curves, with T_c at ~580°C indicating the presence of magnetite. A second inflexion at 350-420°C observed in ash layer of TA and mud-brick of TT can be interpreted as Ti-rich titanomagnetite as a second carrier. IRM acquisition curves (green lines) for all samples show saturations fields <200 mT. The FORC diagrams of oriented cores are generated using a smoothing factor (SF) of 3 and contour interval of 10. All mud-brick and basalt samples have closed inner contours and display narrow vertical spreading indicating the dominance of non-interacting PSD grains. (b) Hysteresis ratios plotted in Day plot modified by Dunlop (2002). Majority of the samples plot above the SD-MD mixing lines but well into the PSD field of the plot.

Figure 3. (a) Stepwise microwave - MW (potsherds), and thermal-Th or alternating field-AF (oriented samples) demagnetisation diagrams. Closed (open) symbols represent the projection of the vector end-points on the horizontal (vertical) plane; values represent microwave power/time in Watt/second, temperature in °C or alternating field in or mT. Normalized intensity decay plots are also shown for the oriented samples. All samples,

except for a partially burnt mud-brick from TA where there is a low-temperature (LT) and a high temperature (HT) component, display a single component demagnetisation diagram decaying to the origin. (b) Comparison of Th and AF demagnetisations using the coordinate bootstrap test (Tauxe, 2010) for randomly selected mud-brick set (KN2).

Figure 4. The characteristic remanent magnetisation (ChRM) directions. The red circles are α_{95} cone of confidence, k is dispersion parameter and D/I is the declination and inclination. For the inclination only sets (TA14-TA18), high-temperature/high coercivity (HT/HC) and low-temperature/low coercivity (LT/LC) components are shown separately.

Figure 5. NRM-TRM plots of one representative example from each sample set and associated orthogonal vector plots in core coordinates. The arrows represent the $pT_{(M)}RM$ checks and the squares are pT_MRM tail checks enabled when applying the Coe protocol on potsherds. Closed (open) circles are accepted (rejected) double heating steps; values represent microwave power/time in Watt/second or temperature in °C. Solid blue (open green) circles on the orthogonal plots are horizontal (vertical) planes and the plots are single component decaying towards the origin.

Figure 6. New (a) declination and (b) inclination data (red) plotted against Geomagia50.v3.2 data (gray), data from Turkey (blue, pink and orange), Cyprus and Israel (green) and the global field models SHA.DIF.14k (green). The insets are data from this study and Ertepinar et al. (2016, 2012) data plotted against PSV curves from Greece and Bulgaria. (c) site mean VADMs of potsherds (red diamonds) and mud-bricks (red circles) along with the data from Geomagia50.v3.2 (gray), the Middle East, Cyprus, Georgia (orange), and Turkey (blue and pink) and the global field model SHA.DIF.14k (green). The sets with only one successful measurement (N=1) are displayed dark green and transparent. The inset shows comparison of the data from this study, Ertepinar et al. (2016, 2012) data and Geomagia50.v3.2 data with modified Poletti et al. (2018) cut-offs.

References

Béguin, A., Filippidi, A., de Lange, G.J., de Groot, L. V., 2019. The evolution of the Levantine Iron Age geomagnetic Anomaly captured in Mediterranean sediments. Earth Planet. Sci. Lett. 511, 55–66. doi:10.1016/j.epsl.2019.01.021

Ben-Yosef, E., Millman, M., Shaar, R., Tauxe, L., Lipschits, O., 2017. Six centuries of geomagnetic intensity variations recorded by royal Judean stamped jar handles. Proc. Natl. Acad. Sci. 114, 2160–2165. doi:10.1073/pnas.1615797114

Ben-Yosef, E., Ron, H., Tauxe, L., Agnon, A., Genevey, A., Levy, T.E., Avner, U., Najjar, M., 2008a. Application of copper slag in geomagnetic archaeointensity research. J. Geophys. Res. Solid Earth 113. doi:10.1029/2007JB005235

Ben-Yosef, E., Tauxe, L., Levy, T.E., Shaar, R., Ron, H., Najjar, M., 2009. Geomagnetic intensity spike recorded in high resolution slag deposit in Southern Jordan. Earth Planet. Sci. Lett. 287, 529–539. doi:10.1016/j.epsl.2009.09.001

Ben-Yosef, E., Tauxe, L., Ron, H., Agnon, A., Avner, U., Najjar, M., Levy, T.E., 2008b. A new approach for geomagnetic archaeointensity research: insights on ancient metallurgy in the Southern Levant. J. Archaeol. Sci. 35, 2863–2879. doi:10.1016/j.jas.2008.05.016

Biggin, A.J., Badejo, S., Hodgson, E., Muxworthy, A.R., Shaw, J., Dekkers, M.J., 2013. The effect of cooling rate on the intensity of thermoremanent magnetization (TRM) acquired by assemblages of pseudo-single domain, multidomain and interacting single-domain grains. Geophys. J. Int. 193, 1239–1249. doi:10.1093/gji/ggt078

Biggin, A.J., Paterson, G.A., 2014. A new set of qualitative reliability criteria to aid inferences on palaeomagnetic dipole moment variations through geological time. Front. Earth Sci. 2, 1–9. doi:10.3389/feart.2014.00024

Bourne, M.D., Feinberg, J.M., Stafford, T.W., Waters, M.R., Lundelius, E., Forman, S.L., 2016. High-intensity geomagnetic field “spike” observed at ca. 3000 cal BP in Texas, USA. Earth Planet. Sci. Lett. 442, 80–92. doi:10.1016/j.epsl.2016.02.051

Brown, M.C., Donadini, F., Korte, M., Nilsson, A., Korhonen, K., Lodge, A., Lengyel, S.N., Constable, C.G., 2015. GEOMAGIA50.v3: 1. general structure and modifications to the archeological and volcanic database. Earth, Planets Sp. 67, 83. doi:10.1186/s40623-015-0232-0

Chauvin, A., Garcia, Y., Lanos, P., Laubenheimer, F., 2000. Paleointensity of the geomagnetic field recovered on archaeomagnetic sites from France. Phys. Earth Planet. Inter. 120, 111–136. doi:10.1016/S0031-9201(00)00148-5

Coe, R.S., 1967. Paleo-intensities of the Earth’s magnetic field determined from Tertiary and Quaternary rocks. J. Geophys. Res. 72, 3247–3262. doi:10.1029/JZ072i012p03247

Coe, R.S., Grommé, S., Mankinen, E.A., 1978. Geomagnetic paleointensities from radiocarbon-dated lava flows on Hawaii and the question of the Pacific nondipole low. J. Geophys. Res. 83, 1740–1756. doi:10.1029/JB083iB04p01740

Day, R., Fuller, M., Schmidt, V.A., 1977. Hysteresis properties of titanomagnetites: Grain-size and compositional dependence. Phys. Earth Planet. Inter. 13, 260–267. doi:10.1016/0031-9201(77)90108-X

de Groot, L. V., Béguin, A., Kosters, M.E., van Rijsingen, E.M., Struijk, E.L.M., Biggin, A.J., Hurst, E.A., Langereis, C.G., Dekkers, M.J., 2015. High paleointensities for the Canary

741 Islands constrain the Levant geomagnetic high 419, 154–167.
742 doi:10.1016/j.epsl.2015.03.020

743 De Marco, E., Tema, E., Lanos, P., Kondopoulou, D., 2014. An updated catalogue of Greek
744 archaeomagnetic data for the last 4500 years and a directional secular variation curve.
745 Stud. Geophys. Geod. 58, 121–147. doi:10.1007/s11200-013-0910-y

746 Dunlop, D.J., 2002. Theory and application of the Day plot (Mrs/Ms versus Hcr/Hc) 2.
747 Application to data for rocks, sediments, and soils. J. Geophys. Res. 107.
748 doi:10.1029/2001JB000487

749 Ertepinar, P., Langereis, C.G., Biggin, A.J., de Groot, L. V., Kulakoğlu, F., Omura, S., Süel,
750 A., 2016. Full vector archaeomagnetic records from Anatolia between 2400 and 1350
751 BCE: Implications for geomagnetic field models and the dating of fires in antiquity. Earth
752 Planet. Sci. Lett. 434, 171–186. doi:10.1016/j.epsl.2015.11.015

753 Ertepinar, P., Langereis, C.G., Biggin, A.J., Frangipane, M., Matney, T., Ökse, T., Engin, A.,
754 2012. Archaeomagnetic study of five mounds from Upper Mesopotamia between 2500
755 and 700 BCE: Further evidence for an extremely strong geomagnetic field ca. 3000
756 years ago. Earth Planet. Sci. Lett. 357–358, 84–98. doi:10.1016/j.epsl.2012.08.039

757 Fisher, R.A., 1953. Dispersion on a sphere. Proc. R. Soc. London 217A, 295–305.

758 Gallet, Y., Butterlin, P., 2015. Archaeological and geomagnetic implications of new
759 archaeomagnetic intensity data from the Early Bronze high terrace 'Massif Rouge' at
760 Mari (Tell Hariri, Syria). Archaeometry 57, 263–276. doi:10.1111/arcm.12112

761 Gallet, Y., D'Andrea, M., Genevey, A., Pinnock, F., Le Goff, M., Matthiae, P., 2014.
762 Archaeomagnetism at Ebla (Tell Mardikh, Syria). New data on geomagnetic field
763 intensity variations in the Near East during the Bronze Age. J. Archaeol. Sci. 42, 295–
764 304. doi:10.1016/J.JAS.2013.11.007

765 Gallet, Y., Genevey, A., Courtillot, V., 2003. On the possible occurrence of "archaeomagnetic
766 jerks" in the geomagnetic field over the past three millennia. Earth Planet. Sci. Lett. 214,
767 237–242. doi:10.1016/S0012-821X(03)00362-5

768 Gallet, Y., Genevey, A., Le Goff, M., Fluteau, F., Ali Eshraghi, S., 2006. Possible impact of
769 the Earth's magnetic field on the history of ancient civilizations. Earth Planet. Sci. Lett.
770 246, 17–26. doi:10.1016/j.epsl.2006.04.001

771 Gallet, Y., Le Goff, M., Genevey, A., Margueron, J., Matthiae, P., 2008. Geomagnetic field
772 intensity behavior in the Middle East between ~3000 BC and ~1500 BC. Geophys. Res.
773 Lett. 35. doi:10.1029/2007GL031991

774 Gallet, Y., Molist Montaña, M., Genevey, A., Clop García, X., Thébault, E., Gómez Bach, A.,
775 Le Goff, M., Robert, B., Nachasova, I., 2015. New Late Neolithic (c. 7000–5000 BC)
776 archeointensity data from Syria. Reconstructing 9000 years of archeomagnetic field
777 intensity variations in the Middle East. Phys. Earth Planet. Inter. 238, 89–103.
778 doi:10.1016/J.PEPI.2014.11.003

779 Games, K.P., 1977. The magnitude of the palaeomagnetic field: a new non-thermal,
780 non-detrital method using Sundried bricks. Geophys. J. R. Astron. Soc. 48, 315–329.
781 doi:10.1111/j.1365-246X.1977.tb03675.x

782 Genevey, A., Gallet, Y., Constable, C.G., Korte, M., Hulot, G., 2008. ArcheoInt: An upgraded
783 compilation of geomagnetic field intensity data for the past ten millennia and its
784 application to the recovery of the past dipole moment. Geochemistry, Geophys.
785 Geosystems 9. doi:10.1029/2007GC001881

786 Genevey, A., Gallet, Y., Margueron, J.-C., 2003. Eight thousand years of geomagnetic field
787 intensity variations in the eastern Mediterranean. J. Geophys. Res. 108.
788 doi:10.1029/2001JB001612

789 Gómez-Paccard, M., Chauvin, A., Albeck, M.E., Zaburlín, M.A., Basso, D.M., Pavón-
790 Carrasco, F.J., Osete, M.L., Campuzano, S.A., 2019. New archeointensity data from
791 NW Argentina (1300–1500 CE). Phys. Earth Planet. Inter. 286, 92–100.
792 doi:10.1016/j.pepi.2018.11.004

793 Hervé, G., Chauvin, A., Lanos, P., 2013. Geomagnetic field variations in Western Europe
794 from 1500BC to 200AD. Part II: New intensity secular variation curve. Phys. Earth
795 Planet. Inter. 218, 51–65. doi:10.1016/j.pepi.2013.02.003

796 Kovacheva, M., Kostadinova-Avramova, M., Jordanova, N., Lanos, P., Boyadzhiev, Y., 2014.
797 Extended and revised archaeomagnetic database and secular variation curves from
798 Bulgaria for the last eight millennia. Phys. Earth Planet. Inter. 236, 79–94.
799 doi:10.1016/J.PEPI.2014.07.002

800 Koymans, M.R., Langereis, C.G., Pastor-Galán, D., van Hinsbergen, D.J.J., 2016.
801 Paleomagnetism.org: An online multi-platform open source environment for
802 paleomagnetic data analysis. Comput. Geosci. 93, 127–137.
803 doi:10.1016/j.cageo.2016.05.007

804 Molina-Cardín, A., Campuzano, S.A., Osete, M.L., Rivero-Montero, M., Pavón-Carrasco,
805 F.J., Palencia-Ortas, A., Martín-Hernández, F., Gómez-Paccard, M., Chauvin, A.,
806 Guerrero-Suárez, S., Pérez-Fuentes, J.C., McIntosh, G., Catanzariti, G., Sastre Blanco,
807 J.C., Larrazabal, J., Fernández Martínez, V.M., Álvarez Sanchís, J.R., Rodríguez-
808 Hernández, J., Martín Viso, I., Garcia i Rubert, D., 2018. Updated Iberian
809 Archeomagnetic Catalogue: New Full Vector Paleosecular Variation Curve for the Last
810 Three Millennia. Geochemistry, Geophys. Geosystems 19, 3637–3656.
811 doi:10.1029/2018GC007781

812 Mullender, T.A.T., van Velzen, A.J., Dekkers, M.J., 1993. Continuous drift correction and
813 separate identification of ferrimagnetic and paramagnetic contributions in
814 thermomagnetic runs. Geophys. J. Int. 114, 663–672. doi:10.1111/j.1365-
815 246X.1993.tb06995.x

816 Nachasova, I.E., Burakov, K.S., 2009. Variation of the intensity of the Earth's magnetic field
817 in Portugal in the 1st millennium BC. Izv. Phys. Solid Earth 45, 595–603.
818 doi:10.1134/s1069351309070040

819 Odah, H., Hussain, A.G., Hoffmann, V., Soffel, H.C., El-Gamili, M., Deebes, H., 2001. Effect
820 of magnetic anisotropy on the experimentally determined palaeointensity of the
821 geomagnetic field. Earth, Planets Sp. 53, 363–371. doi:10.1186/BF03352393

822 Paterson, G.A., 2011. A simple test for the presence of multidomain behavior during
823 paleointensity experiments. J. Geophys. Res. Solid Earth 116, 1–12.
824 doi:10.1029/2011JB008369

825 Paterson, G.A., Tauxe, L., Biggin, A.J., Shaar, R., Jonestrask, L.C., 2014. On improving the
826 selection of Thellier-type paleointensity data. Geochemistry, Geophys. Geosystems 15,
827 1180–1192. doi:10.1002/2013GC005135

828 Pavon-Carrasco, F.J., Osete, M.L., Torta, J.M., De Santis, A., 2014. A geomagnetic field
829 model for the Holocene based on archaeomagnetic and lava flow data. Earth Planet.
830 Sci. Lett. 388, 98–109. doi:10.1016/j.epsl.2013.11.046

831 Poletti, W., Biggin, A.J., Trindade, R.I.F., Hartmann, G.A., Terra-Nova, F., 2018. Continuous
832 millennial decrease of the Earth's magnetic axial dipole. Phys. Earth Planet. Inter. 274,
833 72–86. doi:10.1016/J.PEPI.2017.11.005

834 Riisager, P., Riisager, J., 2001. Detecting multidomain magnetic grains in Thellier
835 palaeointensity experiments. Phys. Earth Planet. Inter. 125, 111–117.

836 Roberts, A.P., Pike, C.R., Verosub, K.L., 2000. First-order reversal curve diagrams: A new
837 tool for characterizing the magnetic properties of natural samples. J. Geophys. Res.
838 105, 461–475. doi:10.1029/2000JB900326

839 Roberts, A.P., Tauxe, L., Heslop, D., Zhao, X., Jiang, Z., 2018. A Critical Appraisal of the
840 "Day" Diagram. J. Geophys. Res. Solid Earth 123, 2618–2644.
841 doi:10.1002/2017JB015247

842 Rogers, J., Fox, J.M.W., Aitken, M.J., 1979. Magnetic anisotropy in ancient pottery. Nature
843 277, 644–646.

844 Selkin, P.A., Tauxe, L., 2000. Long-term variations in palaeointensity. Philos. Trans. R. Soc.
845 A Math. Phys. Eng. Sci. 358, 1065–1088. doi:10.1098/rsta.2000.0574

846 Shaar, R., Ben-Yosef, E., Ron, H., Tauxe, L., Agnon, A., Kessel, R., 2011. Geomagnetic field
847 intensity: How high can it get? How fast can it change? Constraints from Iron Age
848 copper slag. Earth Planet. Sci. Lett. 301, 297–306. doi:10.1016/j.epsl.2010.11.013

849 Shaar, R., Ron, H., Tauxe, L., Kessel, R., Agnon, A., Ben-Yosef, E., Feinberg, J.M., 2010.
850 Testing the accuracy of absolute intensity estimates of the ancient geomagnetic field
851 using copper slag material. Earth Planet. Sci. Lett. 290, 201–213.
852 doi:10.1016/j.epsl.2009.12.022

853 Shaar, R., Tauxe, L., Ben-Yosef, E., Kassianidou, V., Lorentzen, B., Feinberg, J.M., Levy,
854 T.E., 2015. Decadal-scale variations in geomagnetic field intensity from ancient Cypriot
855 slag mounds. Geochemistry, Geophys. Geosystems 16, 195–214.
856 doi:10.1002/2014GC005455

857 Shaar, R., Tauxe, L., Goguitchaichvili, A., Devidze, M., Licheli, V., 2017. Further evidence of
858 the Levantine Iron Age geomagnetic anomaly from Georgian pottery. Geophys. Res.
859 Lett. 44, 2229–2236. doi:10.1002/2016GL071494

860 Shaar, R., Tauxe, L., Ron, H., Ebert, Y., Zuckerman, S., Finkelstein, I., Agnon, A., 2016.
861 Large geomagnetic field anomalies revealed in Bronze to Iron Age archeomagnetic data
862 from Tel Megiddo and Tel Hazor, Israel. Earth Planet. Sci. Lett. 442, 173–185.
863 doi:10.1016/j.epsl.2016.02.038

864 Stillinger, M.D., Feinberg, J.M., Frahm, E., 2015. Refining the archaeomagnetic dating curve
865 for the Near East: New intensity data from Bronze Age ceramics at Tell Mozan, Syria. J.
866 Archaeol. Sci. 53, 345–355. doi:10.1016/j.jas.2014.10.025

867 Tauxe, L., 2010. Essentials of Paleomagnetism. Univ. of California Press, Berkeley.

868 Tauxe, L., Staudigel, H., 2004. Strength of the geomagnetic field in the cretaceous normal
869 superchron: New data from submarine basaltic glass of the Troodos Ophiolite.
870 Geochemistry, Geophys. Geosystems 5. doi:10.1029/2003GC000635

871 Tema, E., Hedley, I., Fasnacht, W., Peege, C., 2018. Insights on the geomagnetic secular
872 variation in the Eastern Mediterranean: First directional data from Cyprus. Phys. Earth
873 Planet. Inter. 285, 1–11. doi:10.1016/J.PEPI.2018.10.001

874 Tema, E., Kondopoulou, D., 2011. Secular variation of the Earth's magnetic field in the
875 Balkan region during the last eight millennia based on archaeomagnetic data. Geophys.
876 J. Int. 186, 603–614. doi:10.1111/j.1365-246X.2011.05088.x

877 Thellier, E., Thellier, O., 1959. Sur l'intensité du champ magnétique terrestre dans le passé
878 historique et geologique. Ann. Geophys. 15, 285–378.

879 Yang, S., Shaw, J., Rolph, T., 1993. Archaeointensity Studies of Peruvian Pottery-from 1200
880 B.C. to 1800 A.D. J. Geomagn. Geoelectr. 45, 1193–1207.

881 Yu, Y., 2011. Importance of cooling rate dependence of thermoremanence in paleointensity
882 determination. J. Geophys. Res. Solid Earth 116. doi:10.1029/2011JB008388

883 Yu, Y., Dunlop, D.J., 2003. On partial thermoremanent magnetization tail checks in Thellier
884 paleointensity determination. J. Geophys. Res. 108. doi:10.1029/2003JB002420

885 Yu, Y., Tauxe, L., Genevey, A., 2004. Toward an optimal geomagnetic field intensity
886 determination technique. Geochemistry, Geophys. Geosystems 5.
887 doi:10.1029/2003GC000630

888 Yutsis-Akimova, S., Gallet, Y., Amirov, S., 2018a. Rapid geomagnetic field intensity
889 variations in the Near East during the 6th millennium BC: New archeointensity data from
890 Halafian site Yarim Tepe II (Northern Iraq). Earth Planet. Sci. Lett. 482, 201–212.
891 doi:10.1016/J.EPSL.2017.11.013

892 Yutsis-Akimova, S., Gallet, Y., Petrova, N., Nowak, S., Le Goff, M., 2018b. Geomagnetic field
893 in the Near East at the beginning of the 6th millennium BC: Evidence for alternating
894 weak and strong intensity variations. Phys. Earth Planet. Inter. 282, 49–59.
895 doi:10.1016/J.PEPI.2018.07.002

896

Figure1

Click here to download Figure: Figure 1_Rev1.pdf

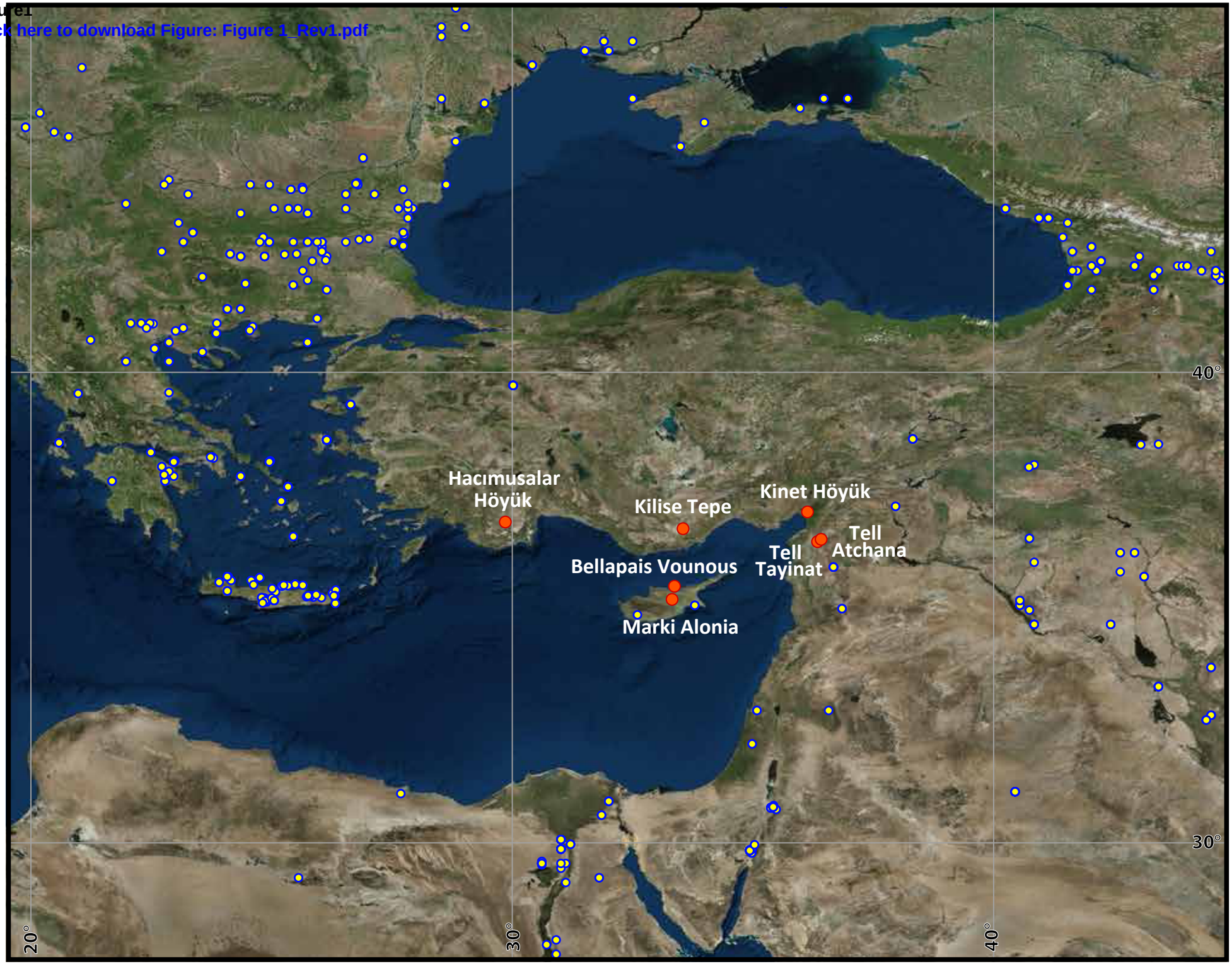

Figure 1

Figure2a

Click here to download Figure: Figure 2a_Rev1.pdf

POTSHERDS

ORIENTED CORES

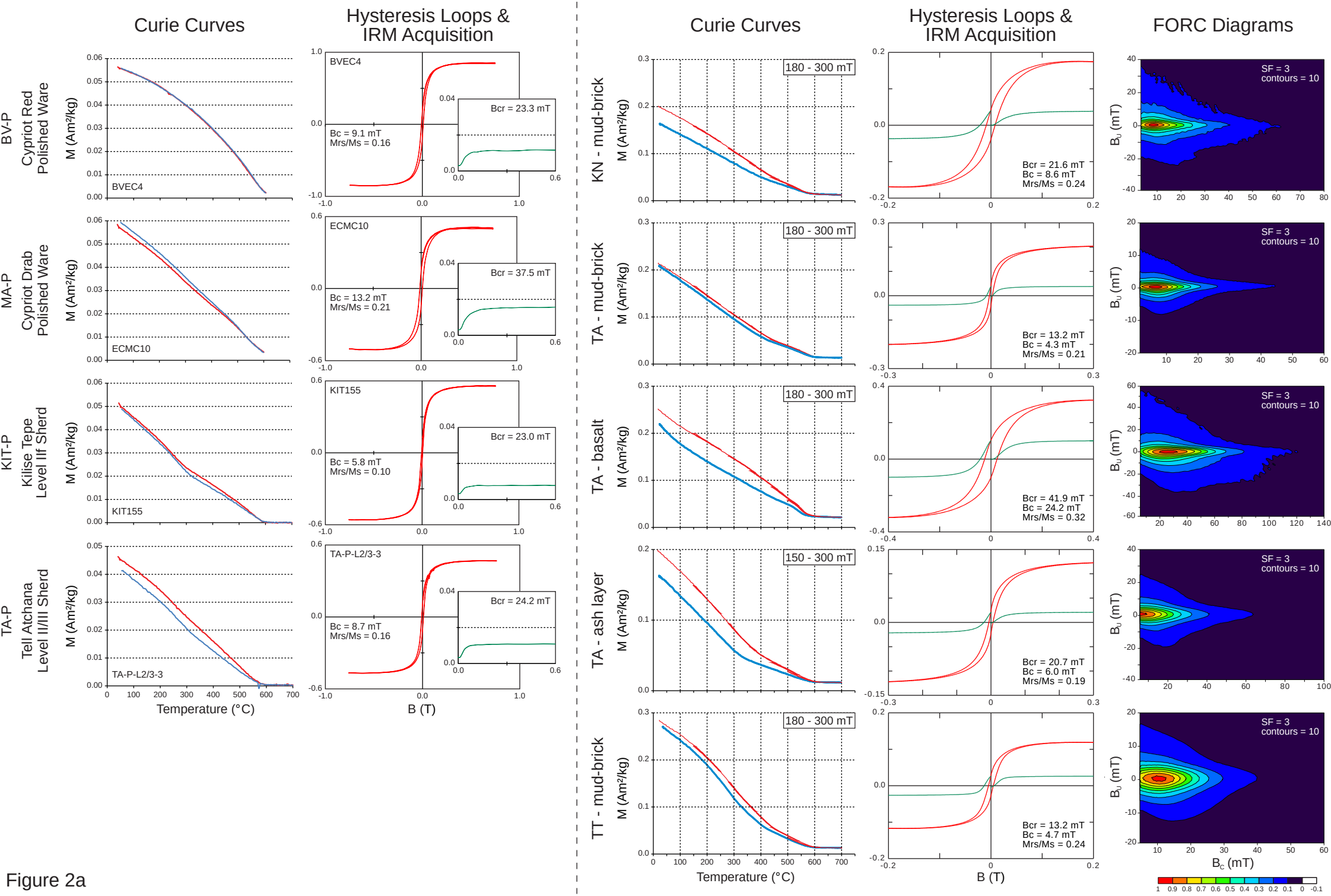

Figure 2a

Figure2b

Click here to download Figure: Figure 2b_Rev1.pdf

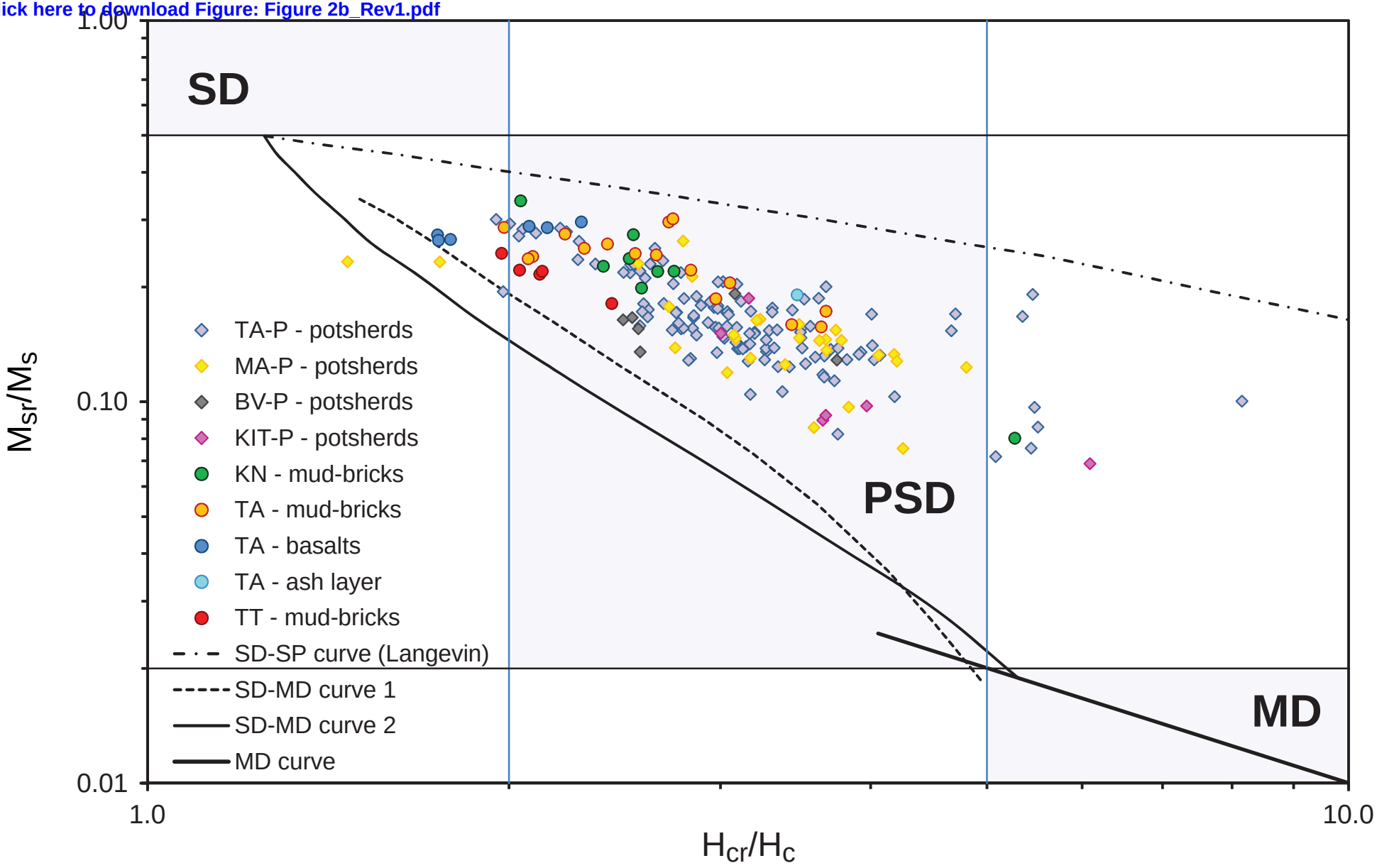

Figure 2b

Figure3a
Click here to download Figure: Figure 3a_Rev2.pdf

Oriented samples (for both directions and intensity)

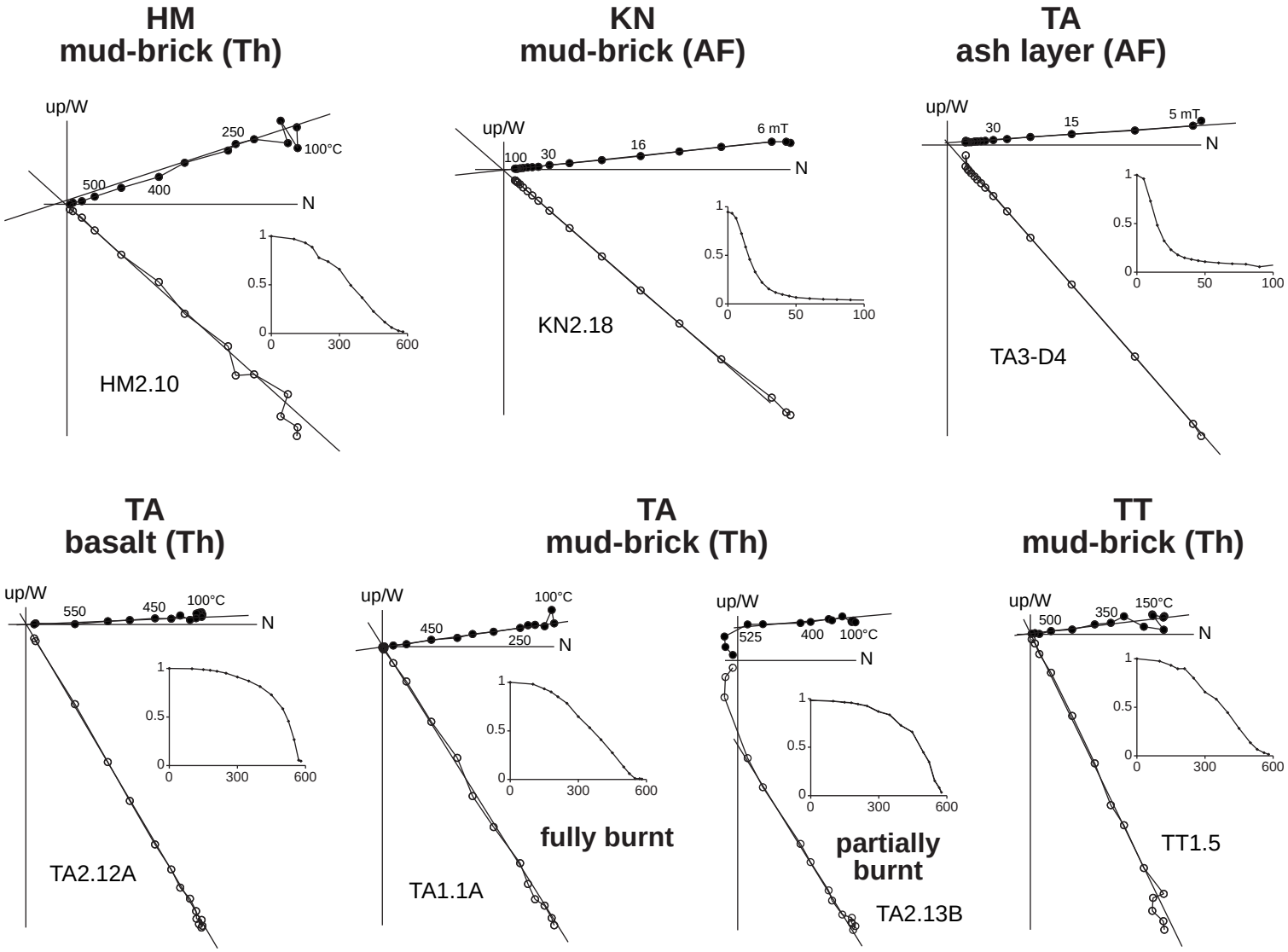

Potsherds (for archaeointensity)

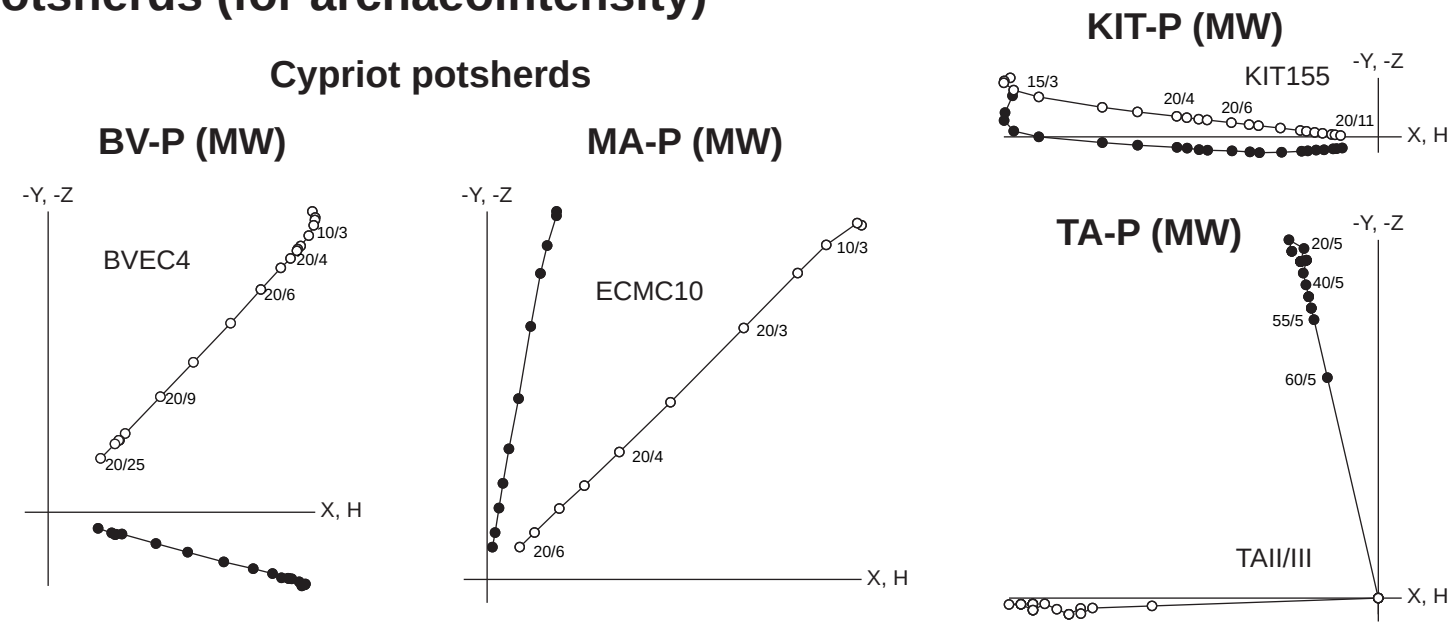

Figure 3a

Figure3b

Click here to download Figure: Figure 3b_Rev1.pdf

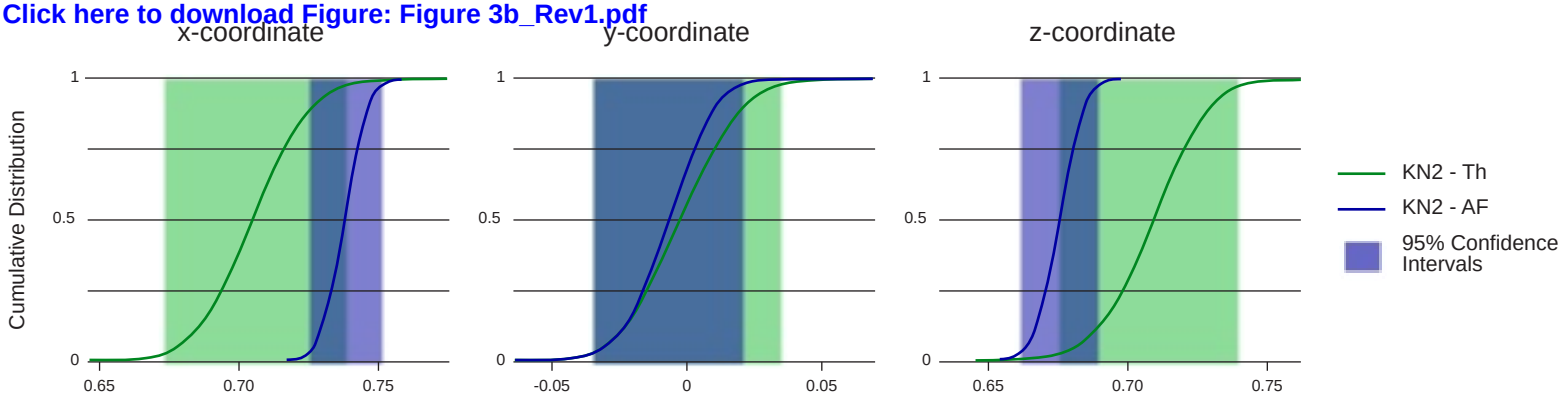

Figure 3b

Figure4

Click here to download Figure: Figure 4_Rev1.pdf

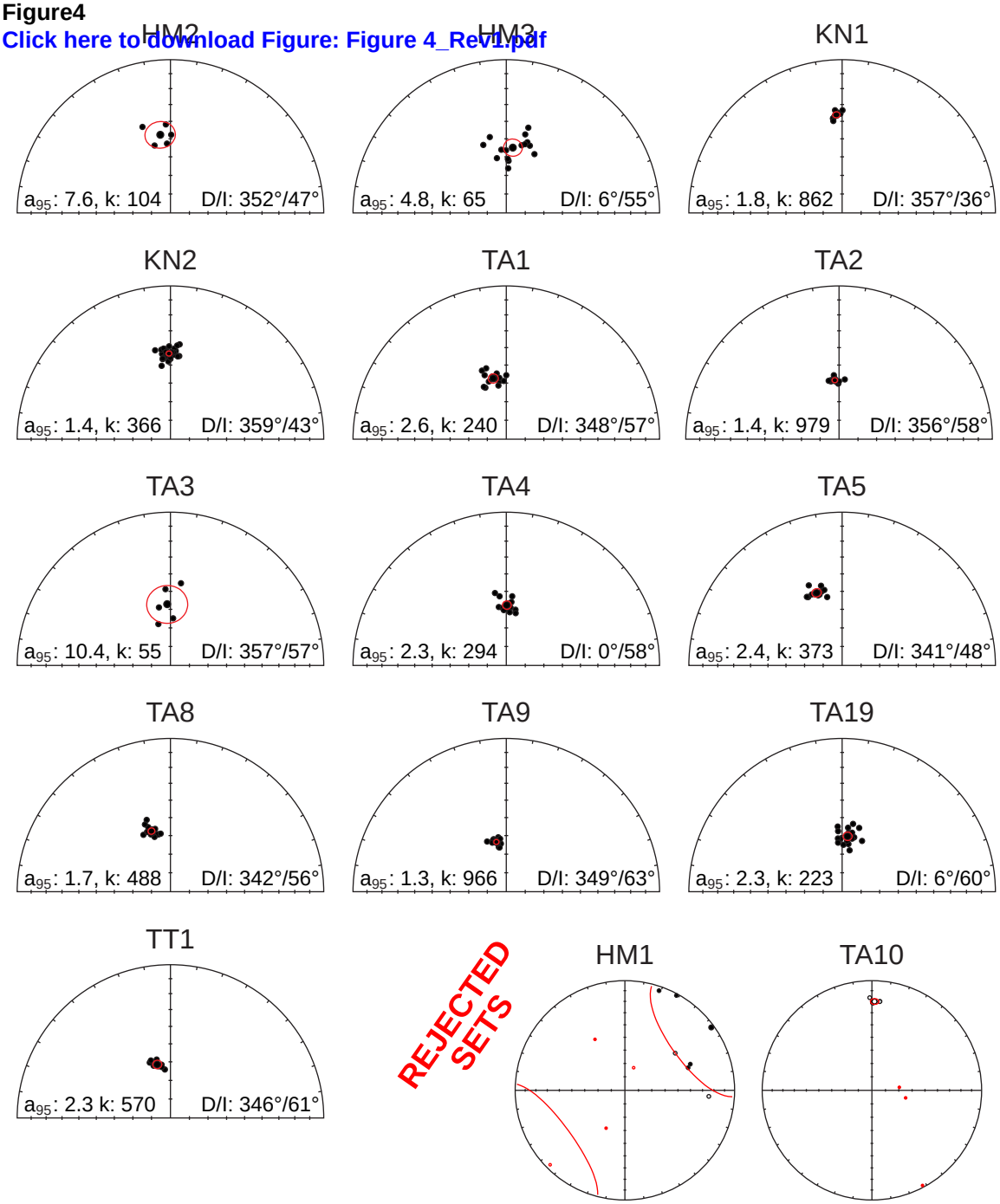

TA PAVEMENT BRICKS

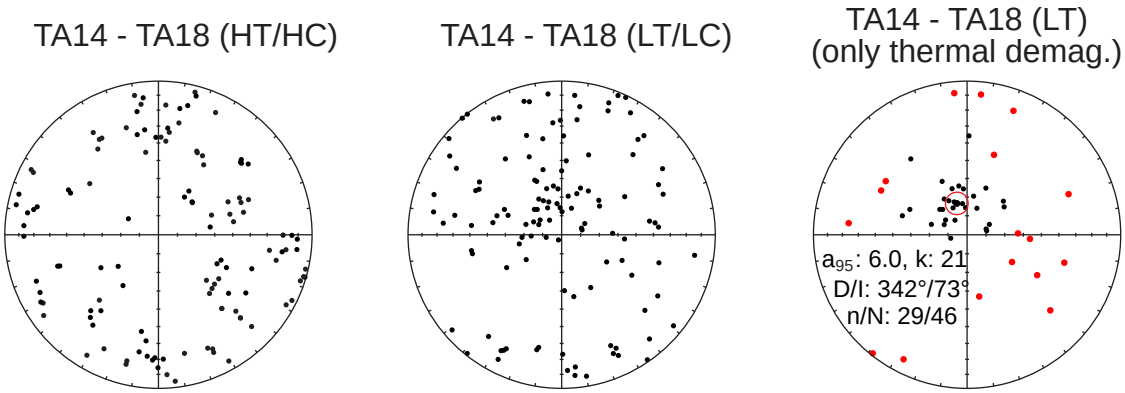

Figure 4

Figure5

Click here to download Figure: Figure 5_Rev1.pdf

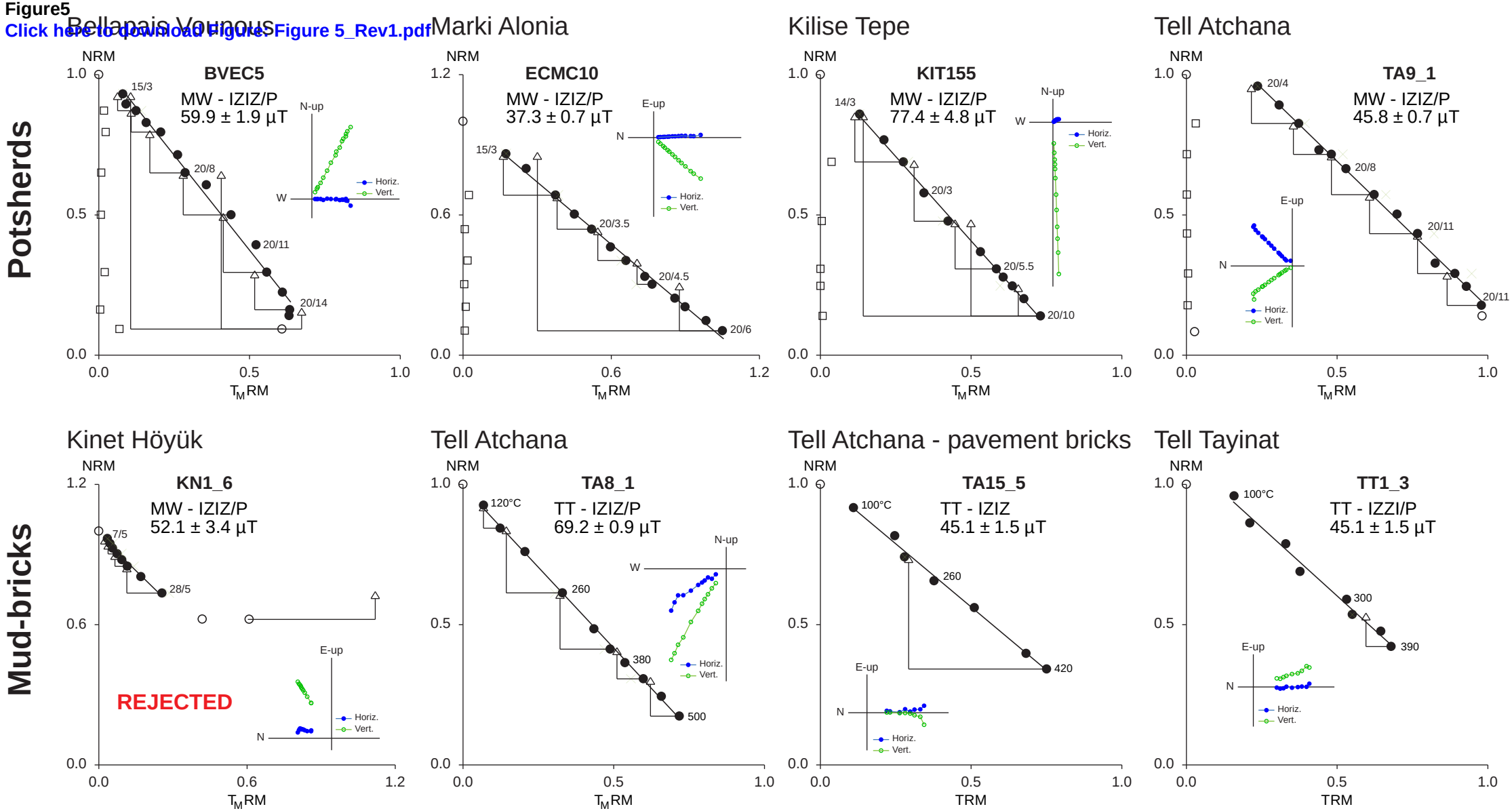

Figure 5

Figure6a

Click here to download Figure: Figure6a_Rev1.pdf

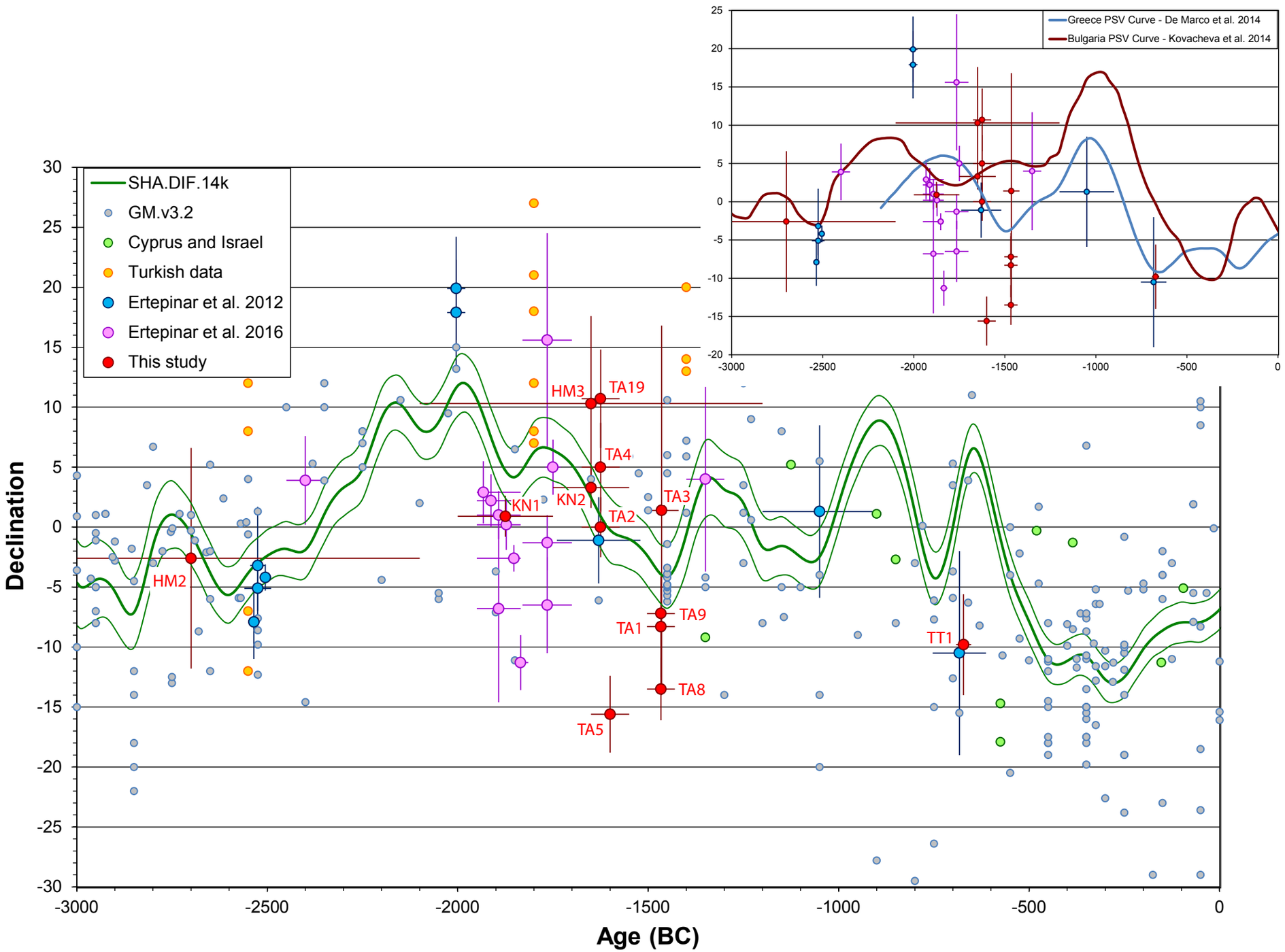

Figure6b

Click here to download Figure: Figure6b_Rev1.pdf

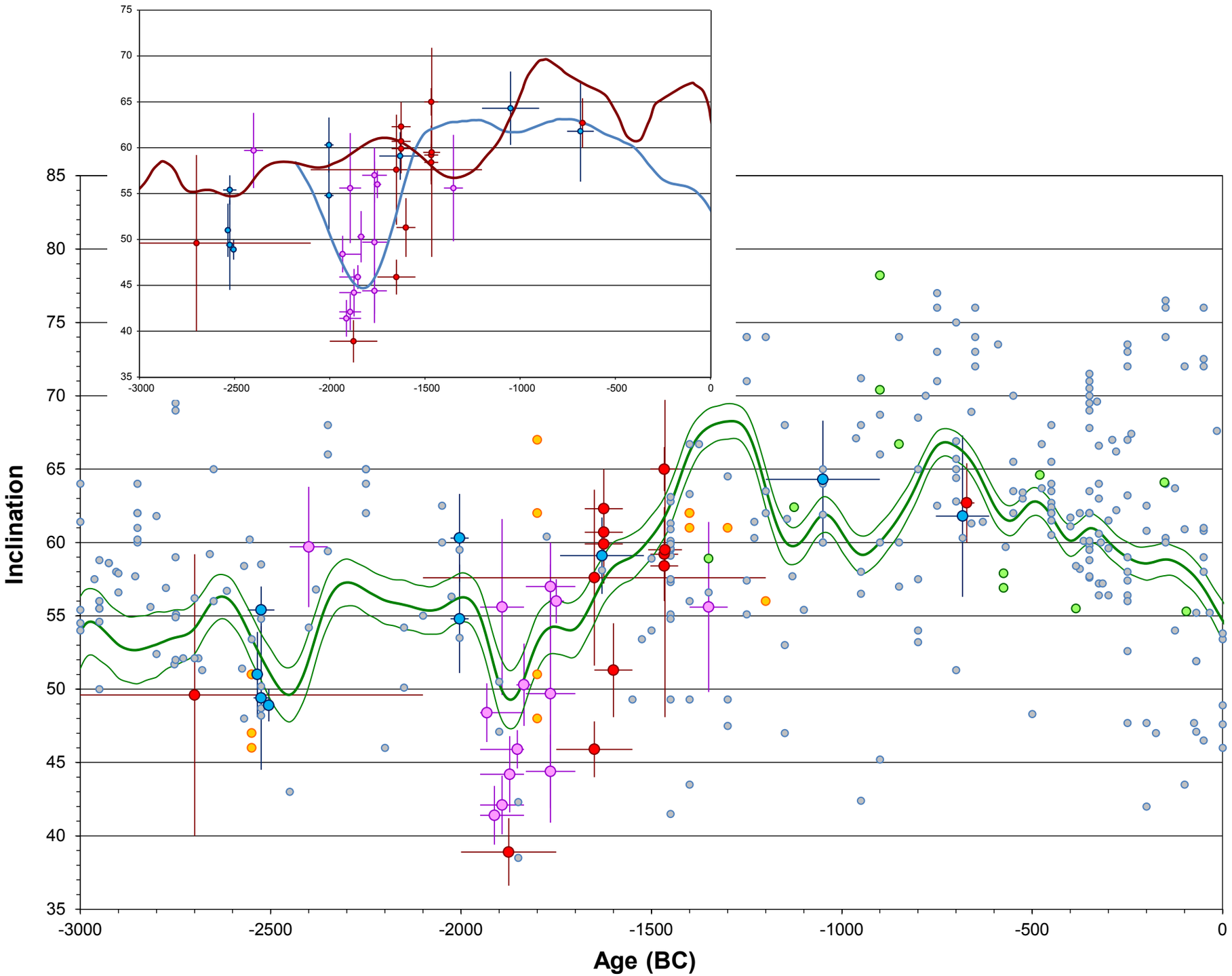

Figure6c

Click here to download Figure: Figure6c_Rev1.pdf

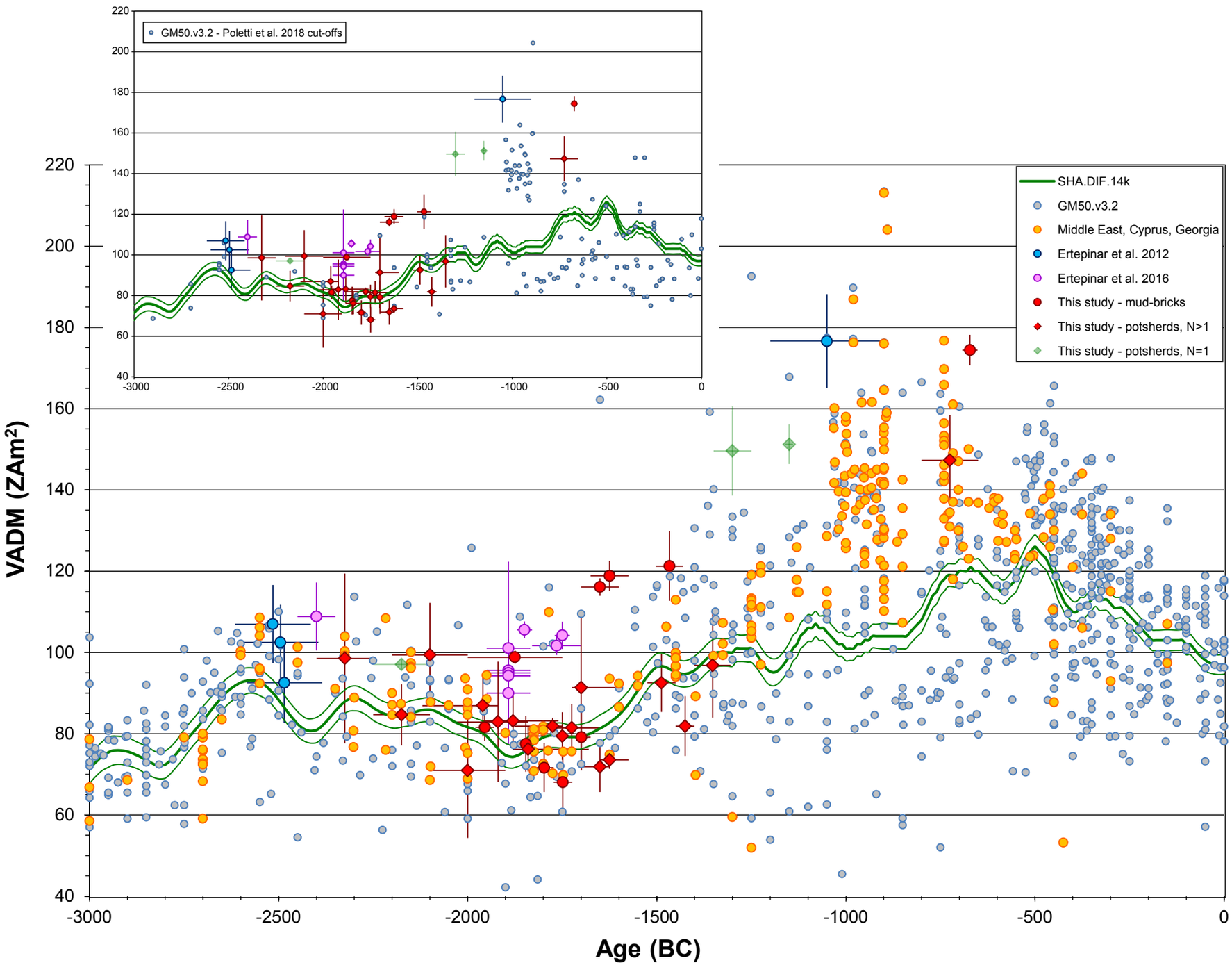

Table1a

Click here to download Table: Table1a_Rev1.xls

Locality	Site	Age (BC)	N
Bellapais Vounous - BV-P *(35°17'57"N, 33°22'28"E)*			
	Early Cypriot I-II	2250 - 2100	6
Marki Alonia - MA-P *(35°01'24"N, 33°19'29"E)*			
	Early Cypriot III/ Middle Cypriot I	2100 - 1900	15
	Early Cypriot I-II	2250 - 2100	1
	Philia Early Cypriot	2400 - 2250	12
Kilise Tepe Höyük - KIT-P *(36°30'09"N, 33°33'13"E)*			
	I/II	1350 - 30	1
	IIa	1350 - 1250	2
	IId	1150 (destruction age)	2
	IIe	1150 - 800	1
	IIf	800 - 650	2
Tell Atchana - TA-P *(36°14'25"N, 36°22'56"E)*			
	II/III	1400 - 1305	9
	IV	1450 - 1400	10
	V	1525 - 1450	10
	VII/VIII	1675 - 1600	9
	IX	1675 - 1600	8
	X	1800 - 1675	8
	XIIa	1800 - 1675	9
	XIIb	1800 - 1675	10
	XIIc	1800 - 1675	8
	XIII	2000 - 1800	9
	XIV	2000 - 1800	7
	XV	2000 - 1800	9
	XVI	2000 - 1800	7
	XVII/XVIII	2200 - 2000	15

Table 1a. Sampling localities with sites, each with a set of N potsherds, for archaeointenty measurements. Ages are based on pottery and relative chronology.

Table1b

Click here to download Table: Table1b_Rev1.xlsx

Locality	Site	Epoch	Age (BC)	Dating Method	Structure	Material
Hacımusalar Höyük *(36°38'32"N, 29°50'11"E)*						
	HM1	Early Iron	1200 - 1000	Relative chronology and stratigraphy	Bricks from a profile	Mud-brick
	HM2	EB	3300 - 2100	Relative chronology and stratigraphy	Clay pit	Clay
	HM3	MB/LB	2100 - 1200	Relative chronology and stratigraphy	Bricks from a profile	Mud-brick
Kinet Höyük *(36°51'13"N, 36°09'26"E)*						
	KN1	MB I	2000 - 1750	Ceramics, archaeological findings	Wall	Mud-brick, serpentinite
	KN2	MB II	1750 - 1550	^{14}C, archaeological findings	Wall	Mud-brick
Tell Atchana *(36°14'25"N, 36°22'56"E)*						
	TA1	LB I	1503 - 1430	Ceramics,^{14}C, relative chronology	Level 4 Palace wall	Mud-brick
	TA2	MB II	1675 - 1600	Ceramics and relative chronology	Level 7 Palace wall	Mud-brick, basalt
	TA3	LB I	1519 - 1420	Ceramics,^{14}C, relative chronology	Furnace floor	Ash layer
	TA4	MB II	1675 - 1600	Ceramics and relative chronology	Level 7 basalt structure	Basalt
	TA5	MB II	1650 - 1550	Ceramics and relative chronology	Hearth	Clay
	TA8	LB I	1503 - 1430	Ceramics,^{14}C, relative chronology	Level 4 Palace wall	Mud-brick
	TA9	LB I	1503 - 1430	Ceramics,^{14}C, relative chronology	Level 4 Palace wall	Mud-brick
	TA10	LB I	1503 - 1430	Ceramics,^{14}C, relative chronology	Level 4 Palace wall	Mud-brick
	TA14	MB II - LB I	1724 - 1675	Relative chronology	Pavement tiles (not *in-situ*)	Mud-brick*
	TA17	MB II - LB I	1773 - 1724	Relative chronology	Palace pavement	Mud-brick*
	TA18	MB II - LB I	1822 - 1773	Relative chronology	Palace pavement	Mud-brick*
	TA16	MB II - LB I	1870 - 1822	Relative chronology	Palace pavement	Mud-brick*
	TA15	MB II - LB I	2040 - 1870	Ceramics,^{14}C, relative chronology	Palace pavement	Mud-brick*
	TA19	MB II	1675 - 1600	Ceramics and relative chronology	Level 7 Palace wall	Basalt
Tell Tayinat *(36°14'54"N, 36°22'33"E)*						
	TT1	Iron Age II	672 (destruction)	Tiglat-Pileser III carving, C14	Wall	Mud-brick

Table 1b. Sampling localities and sites, each with a set of N samples (cores) oriented *in-situ* (except TA14) giving N_{spec} specimens, for both directional and archaeointensity analysis. Mud-bricks are fired during destruction, Mud-bricks* (TA14-18) are baked during manufacture. EB/MB/LB: Early/Middle/Late Bron ^{14}C is radiocarbon dating.

Table2a

Click here to download Table: Table2a_Rev1.xls

Site	Age (BC)	Treatment	n/N	at the site		at Kayseri		k	α_{95}
				Dec	Inc	Dec	Inc		
TA1	1503 - 1430	Th, AF	14/16	-8.0	56.7	-8.3	59.2	239.8	2.6
TA2	1675 - 1600	Th, AF	12/13	0.0	58.3	0.0	60.7	979.1	1.4
TA3	1519 - 1420	AF	5/7	1.3	57.1	1.4	59.5	54.6	10.4
TA4	1675 - 1600	Th, AF	14/20	4.8	57.6	5.0	59.9	293.9	2.3
TA5	1650 - 1550	Th, AF	11/15	-15.1	48.3	-15.6	51.3	373.3	2.4
TA8	1503 - 1430	Th, AF	15/17	-13.1	55.9	-13.5	58.4	487.9	1.7
TA9	1503 - 1430	Th, AF	13/13	-7.0	62.9	-7.2	65.0	965.5	1.3
TA10	1503 - 1430	Th, AF	-	-	-	-	-	-	-
TA19	1675 - 1600	Th, AF	18/20	10.2	60.2	10.7	62.3	222.6	2.3
TT1	672	Th, AF	8/10	-9.5	60.5	-9.8	62.7	570.2	2.3
KN1	2000 - 1750	Th, AF	9/16	1.0	36.0	0.9	38.9	862.1	1.8
KN2	1750 - 1550	Th, AF	28/33	3.4	43.4	3.3	45.9	366.0	1.4
HM1	1200 - 1000	Th, AF	-	-	-	-	-	-	-
HM2	3300 - 2100	Th, AF	5/7	-3.5	47.3	-2.6	49.6	103.5	7.6
HM3	2100 - 1200	Th, AF	15/20	9.9	54.7	10.3	57.6	65.3	4.8

Table 2a. IGRF corrected archaeomagnetic directions from the studied sites. n/N, number of samples accepted over measured; Dec, mean declination; Inc, mean inclination; k, dispersion parameter; α_{95}, 95% confidence cone of mean directions.

Table2b

Click here to download Table: Table2b_Rev1.xlsx

	Site	Age (BC)	Treatment	$n_{(s)}/N_{(s)}$	PI	stdev	PI_{CR}	stdev
POTSHERDS	BV-P (EC I-II)	2250 - 2100	MW	4/5	55.9	5.0	46.4	4.1
	MA-P (EC III/MC I)	2100 - 1900	MW	5/13	49.1	11.5	38.8	9.1
	MA-P (EC I-II)	*2250 - 2100*	*MW*	*1/1*	*63.9*	*---*	*53.0*	*---*
	MA-P (PEC)	2400 - 2250	MW	4/9	62.2	9.6	53.8	11.4
	~~KIT-P level I/II~~	1350 - 30	MW	0/2	---	---	---	---
	KIT-P level II-a	*1350 - 1250*	*MW*	*1/2*	*83.2*	*---*	*---*	*---*
	KIT-P level II-d	*1150*	*MW*	*1/1*	*84.1*	*---*	*---*	*---*
	~~KIT-P level II-e~~	1150 - 800	MW	0/2	---	---	---	---
	KIT-P level II-f	800 - 650	MW	3/6	99.0	6.6	81.9	6.2
	TA-P Level II/III	1400 - 1305	MW	4/9	64.7	8.6	53.7	7.2
	TA-P Level IV	1450 - 1400	MW	7/11	62.2	5.6	45.4	4.1
	TA-P Level V	1525 - 1450	MW	6/8	65.8	5.1	51.3	4.0
	TA-P Level VII/VIII	1675 - 1600	MW	2/6	47.4	1.4	40.8	1.2
	TA-P Level IX	1675 - 1600	MW	5/9	48.0	4.2	39.8	3.5
	TA-P Level X	1800 - 1675	MW	3/9	56.3	10.8	50.6	9.7
	TA-P Level XII-a	1800 - 1675	MW	3/9	51.3	3.6	45.1	3.2
	TA-P Level XII-b	1800 - 1675	MW	7/11	51.8	3.8	44.0	3.3
	TA-P Level XII-c	1800 - 1675	MW	2/6	51.0	1.3	45.4	1.1
	TA-P Level XIII	2000 - 1800	MW	2/8	51.5	3.7	42.2	3.0
	TA-P Level XIV	2000 - 1800	MW	4/8	55.5	4.7	46.1	3.9
	TA-P Level XV	2000 - 1800	MW	2/9	54.1	9.7	46.0	8.2
	TA-P Level XVI	2000 - 1800	MW	4/4	58.8	5.1	48.2	4.2
	TA-P Level XVII/XVIII	2200 - 2000	MW	6/16	51.0	6.6	55.1	7.1
MUD-BRICKS	TA Level IV	1503 - 1430	TT	5/6	67.2	4.8	---	---
	TA Level VII	1675 - 1600	TT	2/3	65.9	2.0	---	---
	~~TA5~~	1650 - 1550	TT	0/1	---	---	---	---
	TA14	1724 - 1675	TT	8/10	43.9	4.6	---	---
	TA15	2040 - 1870	TT	4/5	45.2	1.9	---	---
	TA16	1870 - 1822	TT	7/9	45.0	4.0	43.0	3.8
	TA17	1773 - 1724	TT	7/8	39.2	3.6	37.7	3.5
	TA18	1822 - 1773	TT	9/9	41.9	3.5	39.7	3.3
	TT1	672	MW+TT	2/5	96.7	2.1	---	---
	KN1	2000 - 1750	MW+TT	2/8	55.2	0.9	---	---
	KN2	1750 - 1550	TT	2/2	64.9	1.2	---	---

Table 2b. Archaeointensity results obtained from thermal Thellier & Thellier (TT) and microwave (MW) measurements. $n_{(s)}/N_{(s)}$ is the number of accepted measurements (sherds) over total number of measurements (sherds) analysed, $PI_{ave.}$ is the average paleointensity value of individual samples, stdev is the standard deviation and PI_{CR} is the cooling rate corrected paleointensity result. Sample sets in grey italic have N_s=1 and are deemed not reliable. Strikethrough sample sets gave no result.

Table3

Click here to download Table: Table3_Rev1.xlsx

Site	Lat (°N)	Long (°E)	Age (BC)	dAge	Dec (°)	dDec (°)	Inc (°)	dInc (°)	PI
AT1	38.382	38.361	-1050	150	0.8	7.2	64.0	4.0	100.47
AT-A	38.382	38.361	-2515	100	-3.7	1.1	48.2	1.1	60.84
AT-C	38.382	38.361	-2495	100	-7.4	3.1	50.2	2.9	58.29
AT-D	38.382	38.361	-2485	100	-4.9	1.9	54.8	1.6	52.64
KA1	39.363	33.787	-1765	65	-1.8	2.3	45.1	2.5	58.51
KT1	38.851	35.635	-1750	20	5.0	2.6	56.0	2.0	59.59
KT2	38.851	35.635	-1850	20	-11.3	2.2	50.3	2.0	60.37
KT3	38.851	35.635	-1892.5	57.5	2.9	2.0	48.4	2.0	57.81
KT4	38.851	35.635	-1892.5	57.5	1.0	2.1	42.1	2.6	54.67
KT5	38.851	35.635	-1892.5	57.5	0.2	1.1	44.2	1.3	51.48
KT8	38.851	35.635	-1892.5	57.5	2.2	2.3	41.4	2.8	54.31
KT12	38.851	35.635	-2400	50	3.9	2.3	59.7	1.5	62.26
KT13	38.851	35.635	-1892.5	57.5	-2.6	3.7	45.9	4.1	53.91
KN1	36.854	36.157	-1875	125	1.0	1.7	36.0	2.3	55.20
KN2	36.854	36.157	-1650	50	3.4	1.7	43.4	1.9	64.85
TA-L4	36.240	36.382	-1466.5	36.5	-10.5	3.2	56.3	2.2	67.22
TA-L7	36.240	36.382	-1625	50	0.0	2.5	58.3	1.8	65.90
TT1	36.248	36.376	-672	20	-9.5	4.2	60.5	2.7	96.71

Table 3. IGRF corrected directions (at the site) and archaeointensities, including the full vector resu
from Ertepinar et al. 2012 and 2016.

Supplementary material for online publication only

Click here to download Supplementary material for online publication only: SUPPLEMENTARY MATERIAL_Rev1.docx

FigureS1

Click here to download Supplementary material for online publication only: Fig S1_Rev1.pdf

FigureS2

Click here to download Supplementary material for online publication only: Fig S2_Rev1.pdf

FigureS3

Click here to download Supplementary material for online publication only: Fig S3_Rev1.pdf

FigureS4

Click here to download Supplementary material for online publication only: Fig S4_Rev1.pdf

FigureS5a

Click here to download Supplementary material for online publication only: Fig S5a_Rev1.pdf

FigureS5b

Click here to download Supplementary material for online publication only: Fig S5b_Rev1.pdf

FigureS6

Click here to download Supplementary material for online publication only: Fig S6_Rev1.pdf

FigureS7

Click here to download Supplementary material for online publication only: Fig S7_Rev1.pdf

FigureS8

Click here to download Supplementary material for online publication only: Fig S8_Rev1.pdf

FigureS9

Click here to download Supplementary material for online publication only: Fig S9_Rev1.pdf

TableS1

Click here to download Supplementary material for online publication only: Table S1_Rev1.xlsx

TableS2

Click here to download Supplementary material for online publication only: Table S2_Rev1.xlsx

TableS3a_b

Click here to download Supplementary material for online publication only: Table S3a_b_Rev1.xls

TableS4

Click here to download Supplementary material for online publication only: Table S4_Rev1.xlsx

***Declaration of Interest Statement**

Declaration of interests

☒ The authors declare that they have no known competing financial interests or personal relationships that could have appeared to influence the work reported in this paper.

☐The authors declare the following financial interests/personal relationships which may be considered as potential competing interests: